SANDIA REPORT
SAND2012-3733
Unlimited Release
Printed May 2012

Loop-to-Loop Coupling

Larry K. Warne, Lorena I. Basilio, and William L. Langston, Dept. 1652
Robert A. Salazar, Dept. 1653
Phillip D. Coleman, Larry M. Lucero, and Larry D. Bacon, Dept. 5443

Prepared by
Sandia National Laboratories
Albuquerque, New Mexico 87185 and Livermore, California 94550

Sandia National Laboratories is a multi-program laboratory managed and operated by Sandia Corporation, a wholly owned subsidiary of Lockheed Martin Corporation, for the U.S. Department of Energy's National Nuclear Security Administration under contract DE-AC04-94AL85000.

Sandia National Laboratories

Issued by Sandia National Laboratories, operated for the United States Department of Energy by Sandia Corporation.

Available to DOE and DOE contractors from
U.S. Department of Energy
Office of Scientific and Technical Information
P.O. Box 62
Oak Ridge, TN 37831

Telephone: (865) 576-8401
Facsimile: (865) 576-5728
E-Mail: reports@adonis.osti.gov
Online ordering: http://www.osti.gov/bridge

Available to the public from
U.S. Department of Commerce
National Technical Information Service
5285 Port Royal Rd.
Springfield, VA 22161

Telephone: (800) 553-6847
Facsimile: (703) 605-6900
E-Mail: orders@ntis.fedworld.gov
Online order: http://www.ntis.gov/help/ordermethods.asp?loc=7-4-0#online

SAND2012-3733
Unlimited Release
Printed May 2012

Loop-to-Loop Coupling

Larry K. Warne, Lorena I. Basilio and William L. Langston, Dept. 1652

Robert A. Salazar, Dept. 1653

Phillip D. Coleman, Larry M. Lucero, and Larry D. Bacon Dept. 5443

Sandia National Laboratories
P. O. Box 5800
Albuquerque, NM 87185-1152

Abstract

This report estimates inductively-coupled energy to a low-impedance load in a loop-to-loop arrangement. Both analytical models and full-wave numerical simulations are used and the resulting fields, coupled powers and energies are compared. The energies are simply estimated from the coupled powers through approximations to the energy theorem.

Intentionally Left Blank

Contents

Figures

Tables

Loop-to-Loop Coupling

1 INTRODUCTION

This report considers coupling between wire loops to a low impedance load, which for convenience is taken to have a normalized value of one ohm (power and energy can be scaled to other load values of interest). The problem is carefully formulated to elucidate the basic quantities that influence the coupled energy. The drive or transmitting antenna is taken as either a circular or rectangular loop, while the receiver is taken to be a simple circular loop. The effect of wire leads to the circular loop are also addressed and coupling to the common mode of the leads is considered. An analysis (including both full-wave numerical simulations and an analytic formulation) for a rectangular loop is included since this more closely resembles the preliminary experimental setup. The frequencies are taken to be low enough that circuit (and in some cases transmission line) concepts can often be invoked.

2 TRANSMITTING ANTENNA

Here we consider both a circular and rectangular loop. As previously mentioned, the case of a rectangular-loop transmitter is included to mirror the experimental setup.

2.1 Circular Loop Transmitter in Free Space

For the circular loop it is convenient to use the magnetic vector potential $\underline{A}$, where the magnetic induction $\underline{B}$ and magnetic field intensity $\underline{H}$ are found as

$$\underline{B} = \mu_0 \underline{H} = \nabla \times \underline{A}$$

and $\mu_0 = 4\pi \times 10^{-7}$ H/m is the magnetic permeability of free space. Ignoring displacement currents at low frequencies, Ampere's law

$$\nabla \times \underline{H} = \underline{J}$$

along with the vector identity $\nabla \times \nabla \times \underline{A} = \nabla (\nabla \cdot \underline{A}) - \nabla^2 \underline{A}$ and the choice of the Coulomb gauge $\nabla \cdot \underline{A} = 0$ gives

$$\nabla^2 \underline{A} = -\mu_0 \underline{J}$$

The symmetric current case $J_\varphi (\rho, z)$ scalarizes in cylindrical coordinates (ρ, φ, z) as

$$\left(\nabla^2 - 1/\rho^2\right) A_\varphi = -\mu_0 J_\varphi$$

The potential of a loop of electric current I with radius b at $z = 0$ is [1]

$$A_\varphi = \frac{\mu_0 I}{2\pi} \sqrt{\frac{b}{\rho}} k \left[\left(\frac{2}{k^2} - 1 \right) K(k) - \frac{2}{k^2} E(k) \right]$$

where the complete elliptic integrals are $K(k) = \int_0^{\pi/2} d\theta / \sqrt{1 - k^2 \sin^2 \theta}$ and $E(k) = \int_0^{\pi/2} d\theta \sqrt{1 - k^2 \sin^2 \theta}$ and

$$k = \frac{2\sqrt{\rho b}}{\sqrt{(b+\rho)^2 + z^2}}$$

For the axial component of the magnetic field we have

$$H_z = \frac{1}{\mu_0} \frac{1}{\rho} \frac{\partial}{\partial \rho} (\rho A_\varphi) = \frac{-I}{8\pi \sqrt{b\rho}} k \left[-2K(k) + \left\{ (1 + b/\rho) + \frac{1}{k'^2} (1 - b/\rho) \right\} E(k) \right] \quad (1)$$

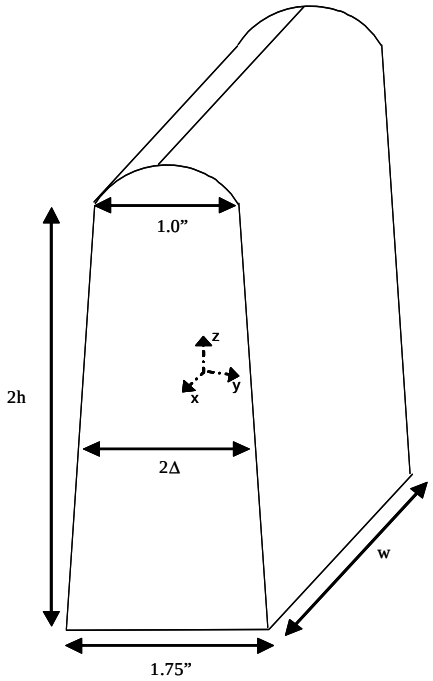

Figure 1. A rectangular loop as used in the test. For analysis, the coordinate system shown is assumed to have an origin between the parallel plates at the center.

For $\rho \to 0$ (along the axis of the circular loop) we have

$$H_\rho(0,z) = 0$$

$$H_z(0,z) = \frac{Ib^2/2}{\left(b^2+z^2\right)^{3/2}} \tag{2}$$

2.2 Thin Rectangular Loop in Free Space

In the initial experimental setup, a strip was bent to form a thin rectangular loop [2]. The rectangular loop geometry is shown in Fig. 1. The motivation in this section is to arrive at a simple closed-form expression for the magnetic field generated by the rectangular loop and ultimately understand the energy coupling between this particular transmitter and a circular loop receiver. For this transmitter case, it is convenient to use the magnetic scalar potential ϕ_m. The rectangular loop, if the gap between the two conducting strips is taken to be quite thin, can be modeled as a pair of magnetic line charges located, respectively, at the inlet and outlet of the thin loop. The field is then found from the gradient of the magnetic scalar potential as

$$\underline{H} = -\nabla\phi_m$$

where a magnetic charge density ρ_m is assumed and from Gauss's law

$$\nabla \cdot \underline{B} = \rho_m$$

Thus we can write

$$\nabla^2\phi_m = -\rho_m/\mu_0$$

and

$$\phi_m(\underline{r}) = \mu_0 \int_V \rho_m(\underline{r}') \frac{dV'}{4\pi\left|\underline{r}-\underline{r}'\right|}$$

The loop portion can be modeled by means of two magnetic line charges $\pm q_m$ of finite length $2h$ and positioned at $x = \pm w/2$ to yield

$$\phi_m = \frac{q_m}{4\pi\mu_0} \ln \left[\frac{z+h+\sqrt{(z+h)^2+(x-w/2)^2+y^2}}{z-h+\sqrt{(z-h)^2+(x-w/2)^2+y^2}} \frac{z-h+\sqrt{(z-h)^2+(x+w/2)+y^2}}{z+h+\sqrt{(z+h)^2+(x+w/2)^2+y^2}} \right]$$

where $\rho = \sqrt{x^2+y^2}$. The x directed field is then

$$(4\pi\mu_0/q_m)\, H_x = \frac{(x-w/2)}{(x-w/2)^2+y^2} \left[\frac{h-z}{\sqrt{(z-h)^2+(x-w/2)^2+y^2}} + \frac{h+z}{\sqrt{(z+h)^2+(x-w/2)^2+y^2}} \right]$$

$$- \frac{(x+w/2)}{(x+w/2)^2+y^2} \left[\frac{h+z}{\sqrt{(z+h)^2+(x+w/2)^2+y^2}} + \frac{h-z}{\sqrt{(z-h)^2+(x+w/2)^2+y^2}} \right] \tag{3}$$

Assuming the rectangular loop is thin with gap $2\Delta << w$ we can calculate the magnetic flux per unit length emanating from the twin stripline as

$$\Phi = L_0 I \tag{4}$$

where the stripline inductance per unit length is L_0 and can be approximated as [3]

$$\pi\mu_0/L_0 \approx \xi + 1 + \ln\left\{2\xi + 1 + 2\ln\left(2\xi+4\right)\right\}\,,\ \xi \geq 1\,,\ (0.5\%\text{ error}) \tag{5}$$

where

$$\xi = \pi w/\left(2\Delta\right)$$

To be consistent with the test we take the dimensions: $w \approx 3$" and a fixed average value $2\Delta \approx (1.75+1)/2$" (this is used for $z = 0$, but a value near 1" was used for observation positions z near the top of the structure) $\xi \approx 6.85$ so that $L_0 \approx 0.289\mu_0$. We note that this rectangular-loop inductance per unit length is smaller than the parallel-plate inductance per-unit length of $\mu_0 2\Delta/w = 0.458\mu_0$. We used an average value $2h \approx 11.5$" to take into account the top circular boundary. We took the absolute observation position z and subtracted the position 0.25" to place the observation point in a symmetric coordinate system (where the structure with the circle is centered at zero) and in reporting the results we return to the absolute coordinate system by adding back the 0.25" shift in z. In general we used linear interpolation to select the spacing $2\Delta = 1" + (1.75" - 1")(h-z)/(2h)$ where here $-h < z < h$ is the symmetric coordinate location. Therefore in Fig. 3 we use an approximation of setting the magnetic charge density to the value at the observation height $q_m(z)$. Thus, the magnetic charge per unit length is set to

$$q_m \approx \Phi \tag{6}$$

For this and the remaining calculations used throughout the report, we had $x = w/2 + d$ and $2h \approx 11.5$". (The distance d corresponds to the sample position from the edge of the rectangular loop, in accordance with the position of the receive antenna.)

As one would expect, as the distance between the transmitting and receiving antenna increases the loop contribution to the magnetic field will decrease and other contributions (for example the feed structure to the loop) may become more important.

2.2.1 Linear Magnetic Charge Density

To account more directly for the variable nature of the gap between conductors (2Δ as shown in Fig. 1), we can also find the field for linear variations of the charge density $q_m(z')$ in a simple form. If we add a linear term, so that the magnetic charge per unit length is

$$q_m(z') = q_m^0 + q_m^1(h-z')$$
$$= q_m^0 + (h-z)\,q_m^1 + q_m^1(z-z')$$

then the identity

$$\int \frac{(z-z')\,dz'}{\sqrt{\rho^2+(z-z')^2}} = -\sqrt{\rho^2+(z-z')^2}$$

can be used on the linear term to give

$$\frac{q_m^1}{4\pi\mu_0}\int_{-h}^{h} \frac{(z-z')\,dz'}{\sqrt{\rho^2+(z-z')^2}} = \frac{q_m^1}{4\pi\mu_0}\left[\sqrt{\rho^2+(h+z)^2}-\sqrt{\rho^2+(h-z)^2}\right]$$

Taking two line sources with opposite signs displaced by $x \pm w/2$ in this case gives

$$\phi_m = \frac{q_m^0+(h-z)\,q_m^1}{4\pi\mu_0}\ln\left[\frac{z+h+\sqrt{(z+h)^2+(x-w/2)^2+y^2}}{z-h+\sqrt{(z-h)^2+(x-w/2)^2+y^2}}\,\frac{z-h+\sqrt{(z-h)^2+(x+w/2)+y^2}}{z+h+\sqrt{(z+h)^2+(x+w/2)^2+y^2}}\right]$$
$$-\frac{q_m^1}{4\pi\mu_0}\left[\sqrt{(x-w/2)^2+y^2+(h-z)^2}-\sqrt{(x-w/2)^2+y^2+(h+z)^2}\right.$$
$$\left.-\sqrt{(x+w/2)^2+y^2+(h-z)^2}+\sqrt{(x+w/2)^2+y^2+(h+z)^2}\right]$$

The x directed field is then

$$(4\pi\mu_0)\,H_x =$$
$$\left\{q_m^0+(h-z)\,q_m^1\right\}\frac{(x-w/2)}{(x-w/2)^2+y^2}\left[\frac{h-z}{\sqrt{(z-h)^2+(x-w/2)^2+y^2}}+\frac{h+z}{\sqrt{(z+h)^2+(x-w/2)^2+y^2}}\right]$$
$$-\left\{q_m^0+(h-z)\,q_m^1\right\}\frac{(x+w/2)}{(x+w/2)^2+y^2}\left[\frac{h+z}{\sqrt{(z+h)^2+(x+w/2)^2+y^2}}+\frac{h-z}{\sqrt{(z-h)^2+(x+w/2)^2+y^2}}\right]$$
$$+q_m^1\,(x-w/2)\left[\frac{1}{\sqrt{(x-w/2)^2+y^2+(h-z)^2}}-\frac{1}{\sqrt{(x-w/2)^2+y^2+(h+z)^2}}\right]$$
$$-q_m^1\,(x+w/2)\left[\frac{1}{\sqrt{(x+w/2)^2+y^2+(h-z)^2}}+\frac{1}{\sqrt{(x+w/2)^2+y^2+(h+z)^2}}\right]$$

This direct analytic solution will also be examined below and compared to numerical simulations of the rectangular loop.

2.2.2 Effective Line Charge

Let us examine the field strength of the stripline arrangement versus the magnetic line charge approximation. We use conformal mapping to find the field for a half plane above a ground plane (approximately representing the edge of the stripline arrangement). By placing the two singularities at $z_1 = -1, 0$ the appropriate Schwarz transformation [4] is

$$\frac{dz}{dz_1} = C_1 z_1^{0/\pi-1}\,(z_1+1)^{2\pi/\pi-1} = C_1\,(1+1/z_1)$$

or

$$z = C_1\,(z_1+\ln z_1)+C_2$$

Now noting that near $z_1 = 0$ we can substitute $z_1 \sim \varepsilon_1 e^{i\theta_1}$, $\varepsilon_1 \to 0$ and write the transformation asymptotically as

$$dz = C_1\,(z_1+1)\,\frac{dz_1}{z_1} \sim C_1 i d\theta_1$$

We want a change $dz \sim i\,(0-\Delta/2)$ for a change $d\theta_1 = (0-\pi)$ at the singular point $z_1 = 0$, so that

$$C_1 = \frac{\Delta}{2\pi}$$

Matching $z_1 = -1$ to $z = i\Delta/2$ gives (note that we use $0 \le \arg z_1 \le \pi$ in the upper half plane)

$$i\Delta/2 = \frac{\Delta}{2\pi}\,(-1+i\pi) + C_2$$

$$C_2 = \frac{\Delta}{2\pi}$$

Thus we have

$$z = \frac{\Delta}{2\pi}\,(1+z_1+\ln z_1)$$

Now we want a magnetic flux per unit length $\Phi/2 = q_m/2$ between the half plane and the plane. We thus take the magnetic scalar potential to be

$$\phi_m = -\frac{1}{\mu_0}\,\mathrm{Re}\,(W)$$

$$\underline{H} = -\nabla\phi_m$$

and the magnetic vector potential to be

$$A_z = \mathrm{Im}\,(W)$$

$$\underline{B} = \mu_0\underline{H} = \nabla\times\underline{A}$$

where

$$W = \frac{q_m}{2\pi}\ln(z_1+1)$$

Using Stokes integral theorem the magnetic flux is given by

$$\Phi = \int_S \underline{B}\cdot\underline{n}dS = \oint \underline{A}\cdot\underline{d\ell}$$

and thus in our two-dimensional case the magnetic flux per unit length is

$$\Phi/2 = A_z\,(x,\Delta/2) - A_z\,(x,0)\ ,\ x<0$$

Using the above representation we see that this implies

$$\Phi/2 = \mathrm{Im}\,[W\,(x+iw/2) - W\,(x+i0)] = \mathrm{Im}\,[W\,(z_1=-1-\varepsilon_1) - W\,(z_1=-1+\varepsilon_1)]$$

$$= \frac{q_m}{2\pi}\,(\pi-0)$$

The scalar potential is therefore

$$\phi_m = -\frac{q_m}{2\pi\mu_0}\ln|z_1+1|$$

The x component of the field is

$$H_x = -\frac{\partial\phi_m}{\partial x} = -\frac{1}{\mu_0}\,\mathrm{Re}\left(\frac{dW}{dz_1}/\frac{dz}{dz_1}\right) = \frac{q_m}{w\mu_0}\,\mathrm{Re}\left[\frac{z_1}{(z_1+1)^2}\right]$$

$$= \frac{q_m}{w\mu_0}\,\mathrm{Re}\left[\frac{1}{(z_1+1)}\left\{1-\frac{1}{(z_1+1)}\right\}\right]$$

Now taking the limit of large $|z|$ and $|z_1|$, the conformal transformation

$$2\pi z/\Delta = 1+z_1+\ln z_1$$

becomes

$$z_1+1 \sim 2\pi z/\Delta - \ln(2\pi z/\Delta - 1)$$

The magnetic field is then

$$H_x \sim \frac{q_m}{2\pi\mu_0}\,\mathrm{Re}\left[\frac{1}{z-\ln(2\pi z/\Delta-1)\,\Delta/(2\pi)}\left(1-\frac{\Delta/(2\pi)}{\{z-\ln(2\pi z/\Delta-1)\,\Delta/(2\pi)\}}\right)\right]$$

$$\sim \frac{q_m}{2\pi\mu_0}\,\mathrm{Re}\left[\frac{1}{z-\{\ln(2\pi z/\Delta-1)-1\}\,\Delta/(2\pi)}\right]$$

On the $x > 0$ axis we thus have

$$H_x(x,0) \sim \frac{q_m/(2\pi\mu_0)}{x - \{\ln(2\pi x/\Delta - 1) - 1\}\Delta/(2\pi)}$$

which shows an increase relative to the magnetic line source value (for $\Delta \to 0$ they coincide)

$$H_x(x,0) \to \frac{q_m}{2\pi\mu_0 x}$$

Thus the magnetic line charge will somewhat underestimate the mutual inductance of the rectangular loop transmitter for closely spaced observation distances x. Hence, even though it is more complicated, we include the next subsection on the vector potential approach.

2.3 Vector Potential Approach

Although we know that a single strip has a current density that varies according to the distribution

$$K_z = \frac{I/\pi}{\sqrt{(w/2)^2 - x^2}}$$

when this strip is near a strip of the same width having an opposite current the current density becomes more uniform. Hence we consider as an approximation a strip of constant current density

$$K_z = I/w$$

of finite length having a vector potential

$$A_z = \frac{\mu_0}{4\pi} K_z \int_{-w/2}^{w/2} \int_{-h}^{h} \frac{dx'dz'}{\sqrt{(x-x')^2 + y^2 + (z-z')^2}}$$

$$= \frac{\mu_0}{4\pi} K_z \int_{x-w/2}^{x+w/2} \int_{z-h}^{z+h} \frac{dudv}{\sqrt{u^2 + y^2 + v^2}}$$

Now using the identity

$$\int \frac{du}{\sqrt{u^2 + a^2}} = \ln\left(u + \sqrt{u^2 + a^2}\right)$$

gives

$$A_z = \frac{\mu_0}{4\pi} K_z \int_{z-h}^{z+h} \ln\left\{(x + w/2) + \sqrt{(x + w/2)^2 + y^2 + v^2}\right\} dv$$
$$-\frac{\mu_0}{4\pi} K_z \int_{z-h}^{z+h} \ln\left\{(x - w/2) + \sqrt{(x - w/2)^2 + y^2 + v^2}\right\} dv$$

The field of interest is

$$\mu_0 H_x = \frac{\partial A_z}{\partial y} - \frac{\partial A_y}{\partial z}$$

Noting that

$$\frac{\partial A_z}{\partial y} = \frac{\mu_0 y}{4\pi} K_z \int_{z-h}^{z+h} \frac{1}{(x + w/2) + \sqrt{(x + w/2)^2 + y^2 + v^2}} \frac{dv}{\sqrt{(x + w/2)^2 + y^2 + v^2}}$$
$$-\frac{\mu_0 y}{4\pi} K_z \int_{z-h}^{z+h} \frac{1}{(x - w/2) + \sqrt{(x - w/2)^2 + y^2 + v^2}} \frac{dv}{\sqrt{(x - w/2)^2 + y^2 + v^2}}$$

for $z + h > 0$ and $z - h < 0$ we have

$$\frac{\partial A_z}{\partial y} = \frac{\mu_0 y}{4\pi} K_z \int_{\sqrt{(x+w/2)^2 + y^2}}^{\sqrt{(x+w/2)^2 + y^2 + (z+h)^2}} \frac{1}{(x + w/2) + \xi} \frac{d\xi}{\sqrt{\xi^2 - (x + w/2)^2 - y^2}}$$

$$-\frac{\mu_0 y}{4\pi}K_z\int_{\sqrt{(x+w/2)^2+y^2+(z-h)^2}}^{\sqrt{(x+w/2)^2+y^2}}\frac{1}{(x+w/2)+\xi}\frac{d\xi}{\sqrt{\xi^2-(x+w/2)^2-y^2}}$$

$$-\frac{\mu_0 y}{4\pi}K_z\int_{\sqrt{(x-w/2)^2+y^2}}^{\sqrt{(x-w/2)^2+y^2+(z+h)^2}}\frac{1}{(x-w/2)+\xi}\frac{d\xi}{\sqrt{\xi^2-(x-w/2)^2-y^2}}$$

$$+\frac{\mu_0 y}{4\pi}K_z\int_{\sqrt{(x-w/2)^2+y^2+(z-h)^2}}^{\sqrt{(x-w/2)^2+y^2}}\frac{1}{(x-w/2)+\xi}\frac{d\xi}{\sqrt{\xi^2-(x-w/2)^2-y^2}}$$

Using the identity [5]

$$\int\frac{dx}{(x+p)\sqrt{R}}=-\int\frac{dt}{\sqrt{c+(b-2pc)\,t+(a-bp+cp^2)\,t^2}}$$

where

$$t=\frac{1}{x+p}$$

$$R=a+bx+cx^2$$

and for $b=0$, $c=1$, $p=(x\pm w/2)$, and $a=-(x\pm w/2)^2-y^2$ and $a+p^2=-y^2$ [5]

$$\int\frac{dx}{(x+p)\sqrt{a+x^2}}=-\int\frac{dt}{\sqrt{1-2pt+(a+p^2)\,t^2}}$$

$$=-\frac{1}{\sqrt{-(a+p^2)}}\arcsin\left[\frac{\left(a+p^2\right)t-p}{\sqrt{-a}}\right]$$

in general gives

$$\frac{\partial A_z}{\partial y}(x,y,z,w,h)=-\frac{\mu_0}{4\pi}K_z$$

$$[F(x+w/2,y,z+h)-F(x+w/2,y,z-h)-F(x-w/2,y,z+h)+F(x-w/2,y,z-h)]$$

where

$$F(x,y,z)=\arcsin\left\{\frac{y^2/\left(x+\sqrt{x^2+y^2+z^2}\right)+x}{\sqrt{x^2+y^2}}\right\}\operatorname{sgn}(y)\operatorname{sgn}(z)$$

Now to calculate the total field of the rectangular loop we take the sum of four pieces by shifting and rotating the coordinates

$$\mu_0 H_x(x,y,z)=\frac{\partial A_z}{\partial y}(x,y-\Delta,z,w,h)-\frac{\partial A_z}{\partial y}(x,y+\Delta,z,w,h)$$

$$+\frac{\partial A_z}{\partial y}(x,z-h,y,w,\Delta)-\frac{\partial A_z}{\partial y}(x,z+h,y,w,\Delta)\qquad(7)$$

One could somewhat rigorously account for the spacing variation by mapping the position of the side strips into nonparallel arrangements, however, if we choose the normal distance to the side strips at the appropriate distance for the observation location being investigated we should end up with a reasonable approximation.

2.4 Comparing Rectangular Loop Numerical Simulation to Preceding Model Results

The analytic treatment of the rectangular-loop antenna (Fig. 1) presented in the preceding section is now compared to a numerical simulation for verification purposes. The numerical simulation is based on EIGER, an integral-equation method-of-moments code. This numerical simulation modeled the metallic conductors of the rectangular loop with a total current injected by four wire sources at the bottom of the loop (the two interior wires included 100 ohm resistors in series with a 1 volt source and the two outer wires included 200 ohm resistors in series with a 1 volt source). Note that we had to boost the frequency in the

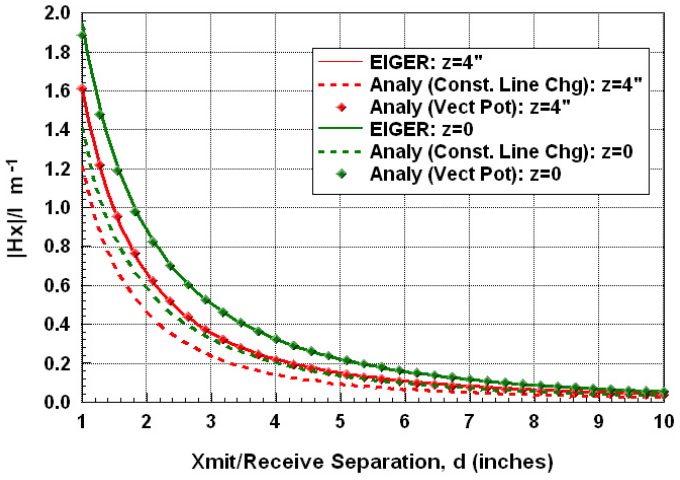

Figure 2. The magnitude of H_x/I generated by a rectangular loop antenna as shown in Fig. 1. The field is sampled at z=4" (red curves) and z=0 (green curves) for various distances measured from the edge of the rectangular loop (d).

simulation to 5.84 MHz to avoid instabilities in the electric field integral equation solution.

Figure 2 shows a comparison between the closed-form analytic expression in (3) and the numerically-simulated result for the magnitude of H_x based on a rectangular transmitting loop. Reasonable agreement between the results is observed as the sample point is varied from $d = 1$" to $d = 10$", although a slight offset is seen between the two sets of data for each sample point z. (Note that two cases for the z-coordinate are considered in the sampling, with $z = 0$ corresponding to the center of the vertical section of the loop and $z = 4$" corresponding to about two inches from the top of the rounded part of the loop.) Also included in Fig. 2 is the analytic solution for the normalized magnetic field when the magnetic vector potential associated with the rectangular loop geometry (7) is carried out. While this approach shows excellent agreement with the numerical simulations (for both $z = 0$ and $z = 4$"), it is important to recognize that it is a much more tedious calculation than the closed-form calculation based on the constant magnetic line charge (3). Note that the results in Fig. 2 have been normalized by the drive-current I, since the calculations are quasistatic and thus the magnetic field of the transmitter loop is instantaneously proportional to the current. For an additional comparison, the analytic and numerical simulation results (for the magnitude of H_x) are plotted in the $x = 4.5$"plane ($d = 3$") in Fig. 3. In this figure an approximation for the magnetic charge density q_m was taken in the analytic solution to have the value corresponding to the value of 2Δ at the observation location z, when z was in the range of $-h < z < h$; outside of this interval it was set to the value at either $z = \pm h$. Reasonable agreement between the analytic and numerical solution is observed. We have also included Fig. 4 when the magnetic line charge has a linearly varying density q_m This comparison is similar to the preceding constant line charge case even though here the spacing variation 2Δ is approximately incorporated into the model from the beginning. Fig. 5 shows the comparison when the magnetic vector potential is used with the same varying spacing 2Δ as used for the constant magnetic line charge. Good agreement between the analytic and numerical solution is observed in this final case.

3 RECEIVING ANTENNA

In this section we consider a simple circular-loop antenna in free-space as the receiver.

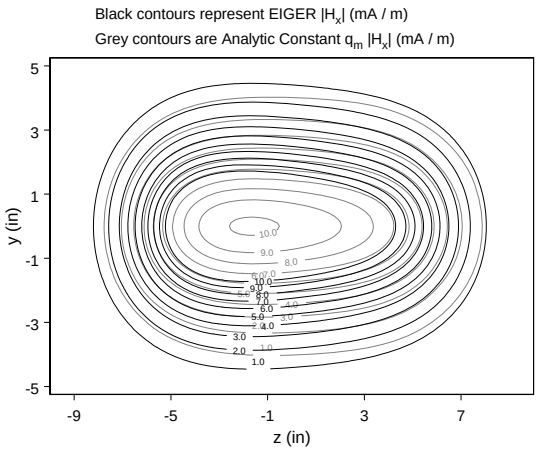

Figure 3. $|H_x|$ plotted across the rectangular loop transmitter along the $x = 4.5$" plane ($d = 3$") for a total drive current of $I = 30$ mA. Results obtained from the analytic formulation and the numerical simulation are included. The analytic curves are from the constant magnetic charge formulas, but we allow the magnetic charge per unit length to be selected from the width corresponding to the observation location.

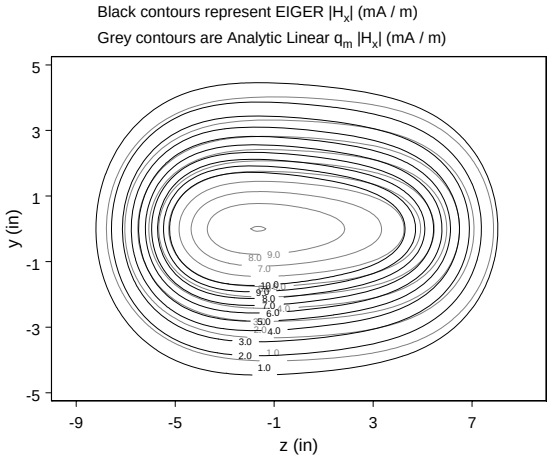

Figure 4. $|H_x|$ plotted across the rectangular loop transmitter along the $x = 4.5$" plane ($d = 3$") for a total drive current of I=30 mA. Results obtained from the analytic formulation and the numerical simulation are included. The analytic curves are from the linear magnetic charge formulas.

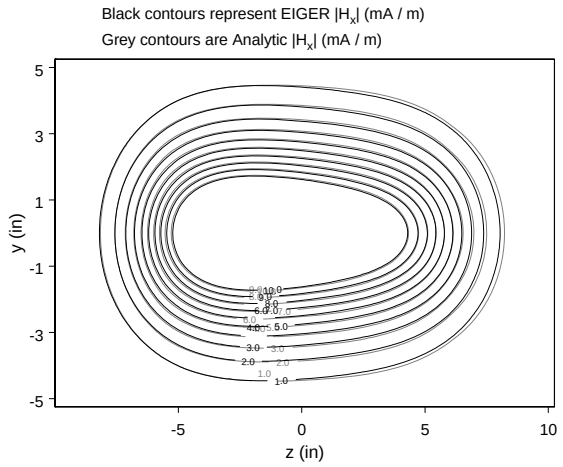

Figure 5. $|H_x|$ plotted across the rectangular loop transmitter along the $x = 4.5$" plane ($d = 3$") for a total drive current of I=30 mA. Results obtained from the analytic formulation and the numerical simulation are included. The analytic curves are from the vector potential formulas.

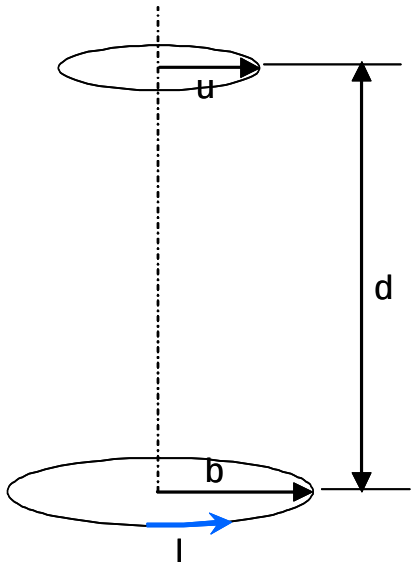

Figure 6. Two circular loop transmit and receive antennas.

3.1 Mutual Inductance & Circuit Picture

The transmitting and receiving circular-loop pair shown in Fig. 6 are analytically treated in this section. The goal here is to derive a closed-form solution for the mutual inductance that can then be used to arrive at a circuit-model expression for the power received at the circular loop due to the drive antenna. Thus, the flux captured by a loop with radius $\rho = u$ and positioned at $z = d$ due to a transmitting loop of current with radius b is

$$\Phi = 2\pi u A_{\varphi}(u, d)$$

and thus the mutual inductance is [1]

$$M = \Phi / I = \mu_0 \sqrt{bu} \left[\left(\frac{2}{k} - k \right) K(k) - \frac{2}{k} E(k) \right] \tag{8}$$

$$k = \frac{2\sqrt{bu}}{\sqrt{d^2 + (u+b)^2}} \tag{9}$$

Note that for $u << b$ we can approximate the coupling by assuming the axial field of the transmitting loop drives the receiving loop

$$M_0 = \pi u^2 \mu_0 H_z(0, d) / I = \frac{\mu_0}{2\pi} \frac{(\pi b^2)(\pi u^2)}{(b^2 + d^2)^{3/2}} \tag{10}$$

To denote the power received by the load, we taken into account a load impedance of $Z_L = R_L + iX_L$ and a loop-antenna impedance equal to Z_a. Thus,

$$P_{rec} = \frac{1}{2} R_L |I_L|^2 = \frac{1}{2} R_L \frac{|V_{oc}|^2}{|Z_a + Z_L|^2} = \frac{1}{2} R_L \frac{|-i\omega M I|^2}{|Z_a + Z_L|^2} \tag{11}$$

where a harmonic-time dependence $e^{-i\omega t}$ is assumed. If we substitute in the preceding approximation for the mutual inductance corresponding to a small-loop receiver (10), then the power received can be written as

$$P_{rec} \sim R_L \frac{(\omega A_r)^2 \mu_0}{|Z_a + Z_L|^2} \frac{1}{2} \mu_0 |H_z(0, d)|^2 = R_L \frac{\eta_1 (k_1 A_r)^2}{|Z_a + Z_L|^2} S_0 \tag{12}$$

where $A_r = \pi u^2$ is the enclosed area by the receiving loop and

$$S_0 = \frac{1}{2}\eta_1 \left|H_z\left(0,d\right)\right|^2 \tag{13}$$

In (12) we have introduced the wavenumber $k_1 = \omega\sqrt{\mu_0\varepsilon_1} = k_0\sqrt{\varepsilon_{r1}}$ in the medium surrounding the loop, where the free space wavenumber $k_0 = \omega\sqrt{\mu_0\varepsilon_0} = \omega/c$. Here c is the free space velocity of light, $\varepsilon_1 = \varepsilon_{r1}\varepsilon_0$ is the permittivity of the medium (ε_{r1} is the relative permittivity of the medium), and $\varepsilon_0 = 8.854$ pF/m is the permittivity of free space. We have also introduced the wave impedance in the medium $\eta_1 = \sqrt{\mu_0/\varepsilon_1} = \eta_0/\sqrt{\varepsilon_{r1}}$, where the intrinsic impedance of free space is $\eta_0 = \sqrt{\mu_0/\varepsilon_0} \approx 120\pi$ ohms. Note that $k_1^2\eta_1^2 = k_0^2\eta_0^2 = \omega^2\mu_0^2$. These quantities will be referred to in the antenna picture to be discussed in Section 3.4.

3.1.1 Loop-Circuit Parameters

At low frequencies we expect the loop inductance to dominate, so the antenna impedance becomes

$$Z_a \sim -i\omega L_a$$

The inductance of a circular loop of radius u and wire radius a is found by evaluating the preceding loop-to-loop mutual inductance on the self-wire surface [1]. Thus,

$$L_a \sim u\mu_0\left[\ln\left(8u/a\right) - 2\right] \approx \frac{P}{2\pi}\mu_0\left[\ln\left(P/a\right) - 1.76\right] \approx 0.199\ \mu\text{H} \tag{14}$$

where again the loop is formed by a $2u = 3$" diameter with 16 gauge wire having $2a = 0.051$". For the right-hand side of (14) we have rewritten the formula in terms of the perimeter $P = 2\pi u$. Note that for a square loop of perimeter P the inductance is [6]

$$L_a \approx \frac{P}{2\pi}\mu_0\left[\ln\left(P/a\right) - 2.16\right]$$

which yields a value similar to the circular loop (of similar area). The resistance of the loop consists of a contribution from radiation (which is negligible at low frequencies, $O\left(10^{-11}\right)$ ohms) [7] of

$$R_{rad} \sim \frac{\eta_1}{6\pi}\left(k_1^2 A_r\right)^2 \tag{15}$$

where again $\eta_1 = \sqrt{\mu_0/\varepsilon_1} = \eta_0/\sqrt{\varepsilon_{r1}}$ is the impedance in the medium containing the loop, $\varepsilon_{r1} = \varepsilon_1/\varepsilon_0$, and $k_1 = \omega\sqrt{\mu_0\varepsilon_1} = k_0\sqrt{\varepsilon_{r1}}$ is the wavenumber in the medium containing the loop. In addition, the total loop resistance includes the metallic losses of the wire making up the loop. Note that at the test frequency of 584 kHz and a copper conductivity of $\sigma \approx 5.8 \times 10^7$ S/m, the skin depth is (assuming the wire is nonmagnetic)

$$\delta = \sqrt{2/\left(\omega\mu_0\sigma\right)} \approx 0.0034 \text{ in}$$

or with $a \approx 0.0255$" we find $\delta/a \approx 0.133$. Hence the resistance associated with the finite wire-conductivity is approximately

$$R_a \sim 2\pi u/\left(2\pi a\delta\sigma\right) \approx 0.012 \text{ ohms}$$

which is significantly smaller than the load $R_L = 1\ \Omega$ and can be ignored. There is also an internal inductive reactance of the wire, which for small skin depths compared to the wire radius, is equal to R_a, but this is negligible compared to the external inductive reactance $X_a = \omega L_a = 0.73\ \Omega$.

The capacitance of an open-circuited loop can be estimated by means of an energy argument [7]. We imagine a current I flowing around the loop (injected near azimuth $\varphi = 0$) and a slowly varying two-wire transmission line (making up the loop) proceeding toward $\varphi = \pi$, where there is a short circuit. The inductance is dominant at low frequencies and the inductive voltage at position φ is then

$$V\left(\varphi\right) = \int_{\varphi}^{\pi} IL\left(\varphi\right) d\left(u\varphi\right) \tag{16}$$

with a two-wire line inductance per unit length of

$$L(\varphi) = \frac{\mu_0}{\pi}\text{Arccosh}\left(\frac{r}{2a}\right) \sim \frac{\mu_0}{\pi}\ln(r/a)$$

[1], [7], with a wire-to-wire spacing of

$$r = 2u\sin\varphi$$

Equation (16) can thus be written as

$$V(\varphi) \sim \frac{\mu_0 uI}{\pi}\left[(\pi-\varphi)\ln(2u/a) + \int_\varphi^\pi \ln(\sin\varphi)\,d\varphi\right]$$
$$\approx V(0)(1-\varphi/\pi)$$

where we have dropped the smaller second term (for a thin wire $u >> a$) in the final expression. The stored electric energy along the line can be written as

$$W_e = \frac{1}{2}C_a|V(0)|^2 = \frac{1}{2}\int_0^\pi C(\varphi)|V(\varphi)|^2\,d(u\varphi) \tag{17}$$

where the wire-to-wire capacitance per unit length is

$$C(\varphi) = \frac{\pi\varepsilon_1}{\text{Arccosh}\left(\frac{r}{2a}\right)} \sim \frac{\pi\varepsilon_1}{\ln(r/a)} \tag{18}$$

Using (18) in (17), we can identify the loop-antenna capacitance as

$$C_a \approx \int_0^\pi C(\varphi)(1-\varphi/\pi)^2\,d(u\varphi)$$

If we approximate $C(\varphi)$ by a constant average value C_{av} then

$$C_a \approx uC_{av}\int_0^\pi (1-\varphi/\pi)^2\,d\varphi = \frac{1}{3}\pi uC_{av} \tag{19}$$

Defining the average by means of averaging the inverse,

$$1/C_{av} = \frac{1}{\pi}\int_0^\pi \frac{d\varphi}{C(\varphi)}$$

we obtain

$$1/C_{av} \sim \frac{1}{\pi}\frac{1}{\pi\varepsilon_1}\int_0^\pi \ln\left(\frac{2u}{a}\sin\varphi\right)d\varphi$$

where the identity

$$\int_0^{\pi/2}\ln(\sin\varphi)\,d\varphi = \frac{1}{2}\int_0^\pi \ln(\sin\varphi)\,d\varphi = -\frac{\pi}{2}\ln(2)$$

yields

$$C_{av} \sim \frac{\pi\varepsilon_1}{\ln(u/a)}$$

Substituting into (19), we end up with

$$C_a \approx \frac{\pi^2\varepsilon_1 u/3}{\ln(u/a)} \approx \varepsilon_{r1}\,(0.272\ p\text{F})$$

for the wire loop of dimensions of $2u = 3$" and $2a = 0.051$". Here again ε_{r1} is the dielectric constant of the medium that surrounds the loop. This capacitance (although it is a low-frequency quantity rather than the reactive quantity near resonance) can be used to get a rough idea of the position of the loop natural resonance $f_{res} \approx \left(2\pi\sqrt{L_aC_a}\right)^{-1} = 684/\sqrt{\varepsilon_{r1}}$ MHz); however, another probably more accurate estimate is based on taking the half circumference to be equal to the length of a quarter-wave resonator

$$\pi u \approx \lambda/4$$

Thus, in air with $u = 1.5$" and $a \approx 0.0255$", we find $\lambda \approx 0.48$ m (or $f_{res} \approx 626$ MHz), whereas the circuit calculation yields 684 MHz. It is important to note that for operating frequencies significantly below resonance this capacitance can be ignored in the circuit model (the antenna inductance dominates).

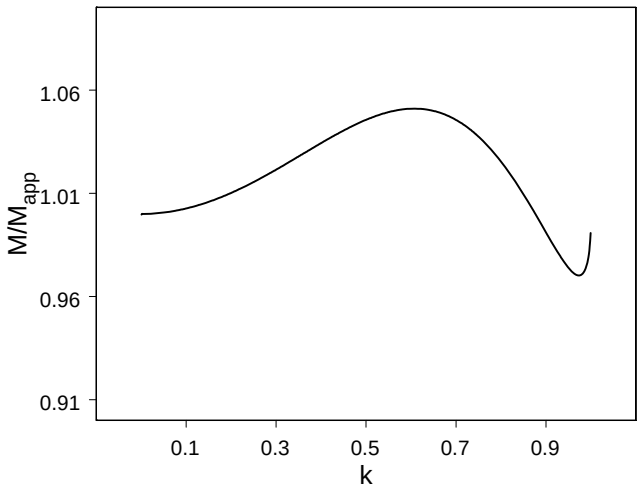

Figure 7. Ratio of exact to approximate expressions for mutual inductance.

3.2 Fit To Mutual Inductance

Here we examine the accuracy of some simple representations for the mutual inductance, which can then be compared to a center-point approximation to the coupled voltage.

3.2.1 Circular Loop To Circular Loop

Fitting the asymptotic limits of the mutual inductance with respect to limits of $k \to 0, 1$ yields an approximate expression $M \approx M_{app}$ (8) with a maximum error of about five percent,

$$M/\left(k^3\mu_0\sqrt{bu}\right) \approx M_{app}/\left(k^3\mu_0\sqrt{bu}\right) = \ln\left(4/\sqrt{1-k^2}\right) - 2 + \sqrt{1-k^2}\,(\pi/16 - 2\ln 2 + 2)$$

where k is defined in (9).

Figure 7 shows the ratio of the exact mutual inductance (8) to the approximate fit (M/M_{app}). With this ratio being very close to one for the full range of k (9), this fit function for the mutual inductance can conveniently be used in place of the more complicated exact expression given in (8). Note that both expressions are specialized to the axial case.

3.2.2 Rectangular Loop To Circular Loop

Fixing the location of the circular receiving loop relative to the rectangular transmitter loop at $x = d + w/2$, the magnetic field generated by the rectangular loop can be written as

$$\left(4\left(\pi\mu_0/L_0\right)/I\right)H_x = \frac{d}{d^2+y^2}\left[\frac{h-z}{\sqrt{(z-h)^2+d^2+y^2}} + \frac{h+z}{\sqrt{(z+h)^2+d^2+y^2}}\right]$$

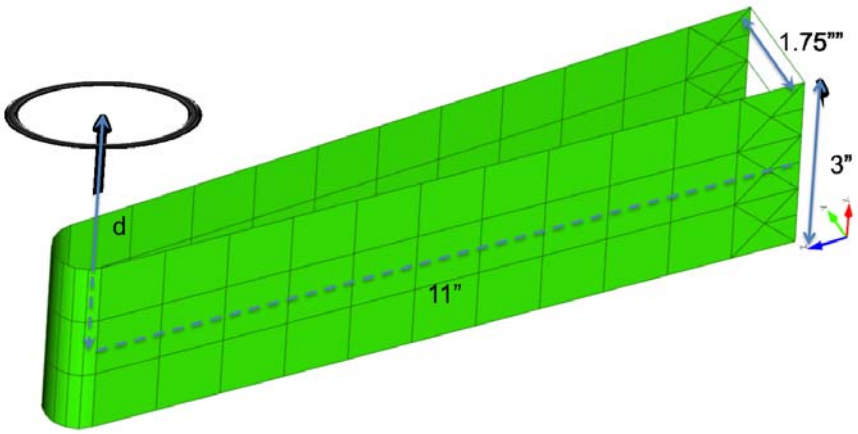

Figure 8. Rectangular transmitter and circular receiver configuration.

$$-\frac{(d+w)}{(d+w)^2+y^2}\left[\frac{h+z}{\sqrt{(z+h)^2+(d+w)^2+y^2}}+\frac{h-z}{\sqrt{(z-h)^2+(d+w)^2+y^2}}\right]$$

The circular loop receiver and rectangular loop transmitter are shown in Fig. 8. Here (3) has been used together with (4) and (6) and, from Section 2.2, we have an approximation to the inductance per unit length, given by (5)

$$\pi\mu_0/L_0 \approx \xi + 1 + \ln\left\{2\xi + 1 + 2\ln\left(2\xi + 4\right)\right\}$$

where

$$\xi = \pi w/\left(2\Delta\right)$$

The flux in the receive loop is

$$\Phi_{tot} = 2\int_{h-u}^{h+u}\int_{0}^{\sqrt{u^2-(z-z_0)^2}} \mu_0 H_x\left(d,y,z\right) dydz$$

Note that this flux integral calculation is constrained to the area within the receive loop, $y^2+\left(z-z_0\right)^2 \leq u^2$.

$$M^{Const} = \Phi_{tot}/I$$

Assuming the dimensions $2u = 3$", $d \approx 3$", $w \approx 3$", $h \approx 5.75$", and fixing the observation point at the receive loop center of $y = 0$ and $z_0 = 5.25$" (this is in the average coordinate system, the absolute location is $z_0 = 5.5$") gives

$$M^{Const} \approx 0.812 \text{ nH}$$

Note that the center-point approximation to the mutual inductance can be written as

$$M_0^{Const} \approx A_r\mu_0 H_x\left(d,0,z_0\right)/I$$

We note that for the dimensions based on the experimental setup

$$M_0^{Const} \approx 0.913 \text{ nH}$$

so the ratio of the preceding accurate integration to the center point value is 0.89; for $d \approx 5$" this ratio becomes 0.95.

The integration of the magnetic field from the preceding linear magnetic charge density approximation gives

$$M^{Lin} \approx 0.846 \text{ nH}$$

whereas the center point value in this case is

$$M_0^{Lin} \approx 0.945 \text{ nH}$$

The more accurate vector potential representation gives

$$M^{Vect} \approx 1.17 \text{ nH}$$

and a center point value of

$$M_0^{Vect} \approx 1.31 \text{ nH}$$

As an additional comparison, integration of the rectangular grid of values from the EIGER simulation using a rectangular pixel approximation gives

$$\Phi_{tot}^{E} = \mu_0 \sum_{mn} A_{rect} H_{mn} \text{ , for } y^2+\left(z-z_0\right)^2 \leq u^2$$

where the rectangular pixel areas are

$$A_{rect} = h_y h_z$$

Here we used $h_y = 10.5"/M$ and $h_z = 20"/N$ with $M+1 = 101 = N+1$ samples taken. The preceding dimensions with $d \approx 3"$ yields (here we included the boundary terms discussed next for greater accuracy)

$$M^{EIG} = \Phi_{tot}^{EIG}/I \approx 1.18 \text{ nH}$$

An interpolated center value gives

$$M_0^{EIG} \approx A_r \mu_0 H_x \left(d, 0, z_0\right)/I \approx 1.31 \text{ nH}$$

so the ratio of integration to center value in the simulation is 0.90. Note that only absolute z values, for example $z_0 = 5.5"$, are used in the numerical simulation and the next subsection.

Boundary Terms To improve the accuracy of the EIGER integration we calculate the boundary areas. We use an approximation by considering the normal to the circle of radius u in the direction of the rectangular pixel center at y_c, z_c. The normal direction to the circle in this direction is then

$$\underline{e}_u = \underline{e}_y \cos\varphi_c + \underline{e}_z \sin\varphi_c$$

where

$$\cos\varphi_c = y_c/\rho$$
$$\sin\varphi_c = \left(z_c - z_0\right)/\rho$$
$$\rho = \sqrt{y_c^2 + \left(z_c - z_0\right)^2}$$

The tangent to the circle is orthogonal to the normal. If we take a vector in the tangent direction as

$$\underline{r} = \left(y - y_c'\right)\underline{e}_y + \left(z - z_c'\right)\underline{e}_z$$

then the slope equation is

$$0 = \underline{e}_u \cdot \underline{r} = \left(y - y_c'\right)\cos\varphi_c + \left(z - z_c'\right)\sin\varphi_c$$

We take a point on this line to be the intersection with the circle of radius u

$$y_c' = u\cos\varphi_c$$
$$z_c' - z_0 = u\sin\varphi_c$$

so the equation for the tangent line is

$$(y)\cos\varphi_c + (z - z_0)\sin\varphi_c = u$$

If we have a rectangular pixel the first check to be made is whether the corresponding tangent line in the center direction intersects the pixel or whether the pixel lies entirely inside the tangent line. Because of the symmetry of the circle we can reflect all pixels to the first quadrant for determination of the area, where then we have $(y)\left|\cos\varphi_c\right| + (z - z_0)\left|\sin\varphi_c\right| = u$, and let us define

$$y_{\min}^{\max} = |y_c| \pm h_y/2$$
$$z_{\min}^{\max} - z_0 = |z_c - z_0| \pm h_z/2$$

The pixel is contained within the circle if

$$(y_{\max})\left|\cos\varphi_c\right| + (z_{\max} - z_0)\left|\sin\varphi_c\right| \le u$$

It is entirely outside the circle if

$$(y_{\min})\left|\cos\varphi_c\right| + (z_{\min} - z_0)\left|\sin\varphi_c\right| \ge u$$

It is on the boundary if

$$(y_{\min})\left|\cos\varphi_c\right| + (z_{\min} - z_0)\left|\sin\varphi_c\right| < u$$
$$(y_{\max})\left|\cos\varphi_c\right| + (z_{\max} - z_0)\left|\sin\varphi_c\right| > u$$

Now if the pixel is on the boundary let us differentiate between four cases. In case I the tangent line intersects the right side boundary at $y = |y_c| + h_y/2 = y_{\max}$, $z = z_2$ and the top of the rectangle at $y = y_2$, $z - z_0 = |z_c - z_0| + h_z/2 = z_{\max} - z_0$, where

$$(y_{\max})\left|\cos\varphi_c\right| + (z_2 - z_0)\left|\sin\varphi_c\right| = u$$
$$(y_2)\left|\cos\varphi_c\right| + (z_{\max} - z_0)\left|\sin\varphi_c\right| = u$$

and here $y_{\min} < y_2 < y_{\max}$, $z_{\min} < z_2 < z_{\max}$. The area to be included in this case (which replaces A_{rect} for this boundary term in the sum) is

$$A = h_y h_z - \frac{1}{2}\left(y_{\max} - y_2\right)\left[\left(z_{\max} - z_0\right) - \left(z_2 - z_0\right)\right] = h_y h_z - \frac{1}{2}\left(y_{\max} - y_2\right)\left(z_{\max} - z_2\right)$$

In case II the tangent line intersects the bottom boundary at $y = y_1$, $z - z_0 = |z_c - z_0| - h_z/2 = z_{\min} - z_0$ and the top boundary at the prior location, where

$$\left(y_1\right)\left|\cos\varphi_c\right| + \left(z_{\min} - z_0\right)\left|\sin\varphi_c\right| = u$$

and here $y_{\min} < y_1 < y_{\max}$, $y_{\min} < y_2 < y_{\max}$. The area in this case is

$$A = \frac{1}{2}\left(y_1 - y_{\min} + y_2 - y_{\min}\right) h_z = \left[\frac{1}{2}\left(y_1 + y_2\right) - y_{\min}\right] h_z$$

In case III the tangent line intersects the left side boundary at $y = |y_c| - h_y/2 = y_{\min}$, $z - z_0 = z_1 - z_0$ and the bottom boundary at the preceding location, where

$$\left(y_{\min}\right)\left|\cos\varphi_c\right| + \left(z_1 - z_0\right)\left|\sin\varphi_c\right| = u$$

and here $y_{\min} < y_1 < y_{\max}$, $z_{\min} < z_1 < z_{\max}$. The area in this case is

$$A = \frac{1}{2}\left(y_1 - y_{\min}\right)\left[z_1 - z_0 - \left(z_{\min} - z_0\right)\right] = \frac{1}{2}\left(y_1 - y_{\min}\right)\left(z_1 - z_{\min}\right)$$

In case IV the tangent line intersects the left side boundary at $y = |y_c| - h_y/2 = y_{\min}$, $z - z_0 = z_1 - z_0$ and the right side boundary at $y = |y_c| + h_y/2 = y_{\max}$, $z = z_2$ where here $z_{\min} < z_1 < z_{\max}$, $z_{\min} < z_2 < z_{\max}$ and the area in this case is

$$A = \frac{1}{2}\left[z_1 - z_0 - \left(z_{\min} - z_0\right) + z_2 - z_0 - \left(z_{\min} - z_0\right)\right] h_y = \left[\frac{1}{2}\left(z_1 + z_2\right) - z_{\min}\right] h_y$$

These results give $M^{EIG} = \Phi_{tot}^{EIG}/I \approx 1.18$ nH ($M_0^{EIG} \approx 1.31$ nH) for $M = 100 = N$. A summary of these values is given in Table 1.

Table 1. Mutual inductance of rectangular transmitting loop and a circular receiving loop of radius u=1.5" shown in Figure 6. A position of z=5.5" and a distance of d=3" are assumed.

d	M_0^{Const}: Center Point	M^{Const}: Integrated Flux
3 in	0.913 nH	0.812 nH
5 in	0.393 nH	0.375 nH
7 in	0.218 nH	0.213 nH
d	M_0^{Lin}: Center Point	M^{Lin}: Integrated Flux
3 in	0.945 nH	0.846 nH
5 in	0.421 nH	0.403 nH
7 in	0.241 nH	0.235 nH
d	M_0^{Vect}: Center Point	M^{Vect}: Integrated Flux
3 in	1.31 nH	1.17 nH
5 in	0.571 nH	0.545 nH
7 in	0.318 nH	0.310 nH
d	M_0^{EIG}: Center Point	M^{EIG}: Integrated Flux
3 in	1.31 nH	1.18 nH

Fig. 9 shows a comparison of the center point magnetic field values from the vector potential representation (which agrees reasonably well with the numerical simulation) versus the magnetic field from the constant magnetic charge model. Also included are the average field values $\langle H_x \rangle$ defined by

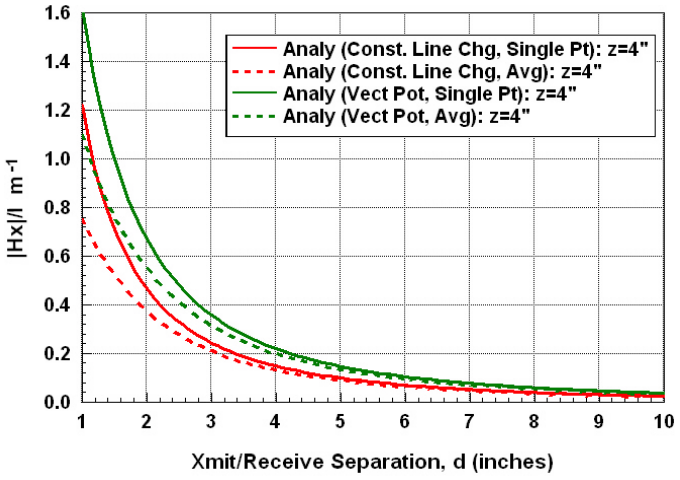

Figure 9. A comparison of the normalized magnetic field H_x/I calculation for the constant magnetic line charge versus the magnetic vector potential approach. Calculations based on a single point evaluation of the field versus an average (integrated) field are also provided. The field is evaluated at z=4" for various distances measured from the edge of the rectangular loop (d).

$$\Phi_{tot} = A_r \mu_0 \langle H_x \rangle$$

where the receiver geometric area in the case of a circular loop of radius $u = 1.5$" is

$$A_r = \pi u^2$$

This illustrates that the use of a center point value from the constant magnetic line charge model can yield reasonable answers for the mutual inductance, particularly when your are not too close to the transmit loop.

3.3 Exact Flux (Or Average Magnetic Field Intensity) Versus Center Point

The open-circuit voltage is

$$V_{oc} = -\frac{d\Phi_{tot}}{dt} = i\omega\Phi_{tot}$$

where the magnetic flux through the receive loop is

$$\Phi_{tot} = \int_{A_r} \mu_0 H_z dA = \int_0^u \int_0^{2\pi} \mu_0 H_z(\rho, \varphi, d)\, \rho d\rho d\varphi \tag{20}$$

(Note here that an axial drive (H_z) field has been assumed. Since in the rectangular-loop analysis, provided above, the drive field was conveniently taken as H_x, H_x would replace H_z in (20).) A center-point approximation of (20) is

$$\Phi_0 \approx A_r \mu_0 H_z(0, \varphi, d)$$

Thus we can define a correction to the center point value in the power (or energy formulas) as

$$F = |\Phi_{tot}/\Phi_0|^2 \tag{21}$$

(note that this is also equal to the square of the ratio of mutual inductances) and then

$$P_{rec} = A_e S_0 F$$

where A_e is the standard antenna quantity of effective area and S_0 is the source power density (or

magnitude of the Poynting vector) evaluated along the axis (center) of the receiving antenna (13). The quantity S_0F is an average (or effective) source power density making use of the square of an integrated (or an average) magnetic field intensity. The antenna effective area definition is discussed in the next section.

It is important to note that the ratio of the received energy computed using the integration (denoted on the plot as 'Avg') to the energy associated with a single-point (at the receive center) calculation is equal to the correction factor F in (21). If we can tolerate the error associated with the approximation of using the center value alone, this allows us to separate transmit loop and receive loop calculations and thereby generalize the results.

3.4 Antenna Picture

As an alternative to the circuit calculation given in (11), the received power can also be written as

$$P_{rec} = A_e S_0 \tag{22}$$

where the effective area is [8]

$$A_e = \frac{\lambda^2}{4\pi} Gqp = R_L \frac{\eta_1 \left(k_1 A_r\right)^2}{\left|Z_a + Z_L\right|^2} p \tag{23}$$

and where G, q, S_0,and p respectively represent the antenna gain G, an impedance mismatch factor q, the magnitude of the incident power density S_0, and a polarization mismatch factor p. It is important to note that (22) with (23) is simply a rewriting of (11) with convenient antenna quantities having been defined. Thus, (22) will yield the same result to the preceding circuit formula for the received power when the center-point value of the transmitter magnetic field is used (12). This restriction can be removed by use of the average discussed in the previous section. If it becomes desirable to estimate coupling at higher frequencies, the antenna picture may sometimes be more convenient as a starting point.

The quantities used for computing the effective area are defined by

$$q = \frac{4R_L R_{rad}}{\left|Z_a + Z_L\right|^2} \tag{24}$$

$$S_0 = \frac{1}{2}\eta_1 \left|\underline{H}\left(0, d\right)\right|^2$$

$$0 \le p = \left|H_z\left(0, d\right) / \underline{H}\left(0, d\right)\right|^2 \le 1$$

where, for an electrically small receiving loop [7], we have

$$G \sim \frac{3}{2}$$

$$R_{rad} \sim \frac{\eta_1}{6\pi}\left(k_1^2 A_r\right)^2$$

3.4.1 Example Antenna Calculation

To calculate the power received for the case of a circular receive loop of $2u = 3$"(of 16 gauge wire) at 1 MHz in free space we have

$$P_{rec} = \frac{\lambda^2}{4\pi} GqS_0 p \sim \frac{\lambda^2}{4\pi}\left(3/2\right) qS_0 p$$

where the receiving antenna properties are given by

$$R_{rad} \approx 8.0 \times 10^{-11} \text{ohms}$$

(15) and for a single-turn receiving loop (circular) (14)

$$L_a \approx 0.199\ \mu\text{H}$$

and

$$Z_a \sim -i\omega L_a \approx -i1.25\ \Omega$$

Assuming a receiving loop load of $Z_L = 1\ \Omega$ then (24) is

$$q \approx 1.25 \times 10^{-10}$$

As one would expect, the impedance mismatch for this small loop at this low frequency is severe and the coupling will be quite low.

Next we assume a transmitting loop of radius $b = 2.5$" (this radius is chosen to keep this circular-loop area consistent with the enclosed area of the rectangular loop used in the test, Fig. 1) and a transmit/receive separation of $d = 3$". For this case, S_0 (13) becomes

$$S_0 = \frac{1}{2}\eta_0 \left(\frac{Ib^2/2}{\left(b^2 + d^2\right)^{3/2}} \right)^2 \approx \left(804\ \mathrm{W/\left(A - m\right)^2} \right) I^2$$

(Here the field generated by a circular-loop transmitter (2) has been used.) Lumping these quantities together to form the received power we have,

$$P_{rec} \approx \frac{\lambda^2}{4\pi} (1.5) \left(1.25 \times 10^{-10}\right) \left(804 I^2\right) (1) \approx I^2 \left(1.08 \times 10^{-3}\ \mathrm{W/A^2}\right)$$

at 1 MHz. (A polarization mismatch factor of $p = 1$ has been assumed).

Increasing the operating frequency to 10 MHz, we have

$$R_{rad} \approx 8.0 \times 10^{-7} \mathrm{ohms}$$

$$Z_a \approx -i12.5\ \Omega$$

$$q \approx 2.04 \times 10^{-8}$$

$$S_0 \approx \left(804\ \mathrm{W/\left(A - m\right)^2} \right) I^2$$

so that

$$P_{rec} \approx I^2 \left(1.8 \times 10^{-3}\ \mathrm{W/A^2}\right)$$

As the frequency increases, the power received remains essentially the same. This can be clearly seen with the received power in the form of (12) since for Z_a dominated by an inductive reactance, the frequency dependence cancels out.

For convenience, the received energies are tabulated below for the circular loop receiver and circular loop transmitter case at various frequencies (away from the receiver resonance). To be consistent with the test setup, a drive current of $I = 140$ kA and $\tau_0 = 7\ \mu$s is assumed in going from the received power calculations to the energy received. As discussed in Section 3.7, for low frequencies we can frequently take

$$W_{rec} = (\tau_0/2)\, P_{rec}$$

Tables 2 and 3 show energy calculations for two different spacings between the transmit and receive antennas.

Table 2. Energy received using a circular loop receiver of u=1.5" and a circular loop transmitter of b=2.5". A transmit/receive seperation of d=3" is assumed

f [MHz]	W_{rec} [J]
0.584	42
1	74
10	121
60	120

In the section below we consider a rectangular-loop transmitting antenna, where we observe that,

Table 3. Energy received using a circular loop receiver of u=1.5" and a circular loop transmitter of b=2.5". A transmit/receive seperation of d=5" is assumed

f [MHz]	W_{rec} [J]
0.584	4.9
1	8.6
10	14
60	14

relative to the circular-transmitter case, the levels of received energy decrease significantly. As mentioned previously, a rectangular-loop transmitter as shown in Fig. 1 is considered here to be consistent with the experimental testing that was ongoing.

3.5 Multiple Turn Loop

If we now consider the same rectangular transmitting loop with a n-turn circular receiver (rather than the 1-turn type as previously considered), (11) is modified to

$$P_{rec}^{n\ turns} = \frac{1}{2}R_L\frac{|nV_{oc}|^2}{\left|n^2Z_a^{(n)}+Z_L\right|^2} = \frac{1}{2}R_L\frac{\eta_0\left(nk_0A_r\right)^2}{\left|n^2Z_a^{(n)}+Z_L\right|^2}\eta_0\left|H_z\left(0,d\right)\right|^2$$

Note that for an n-turn receiving loop, the self-inductance is given by

$$L_a = n^2L_a^{(n)} \approx n^2u\mu_0\left[\ln\left(8u/a_{eq}\right)-2\right] \tag{25}$$

which for $n=3$ and a 3" diameter becomes 1.79 μH when we crudely take $a_{eq}\rightarrow a \approx 0.0255$" (16 gauge wire). However, to more accurately calculate the self-inductance, we note that in addition to the factor of n^2 increase in the inductance associated with the additional turns, the turns have the effect of increasing the effective radius of the wire loop antenna. In the next two sections, two different wire arrangements (resulting in different effective radii) are considered.

3.5.1 Triangular Wire Configuration

If we take the multi-turn wires to be in the configuration of an equilateral triangle (as depicted in Fig. 10a) then the equal current drive results in the proper current distribution to achieve little net flux between the wires when the loop diameter is very large. In this case we can treat the wires as approximately two dimensional and write the vector potential near the wires as

$$A_z = -\frac{\mu_0 I}{2\pi}\sum_{j=0}^{2}\ln\left|x+iy-pe^{ij2\pi/3}/\sqrt{3}\right| + A_0$$

$$= -\frac{\mu_0 I}{2\pi}\ln\sqrt{\left[\left(x-p/\sqrt{3}\right)^2+y^2\right]\left[\left(x+p/\left(2\sqrt{3}\right)\right)^2+\left(y-p/2\right)^2\right]\left[\left(x+p/\left(2\sqrt{3}\right)\right)^2+\left(y+p/2\right)^2\right]} + A_0$$

where p is the spacing between wires (the complex location in this case is $x+iy$).

Now the vector potential on a wire at $x=p/\sqrt{3}+a$ and $y=0$ for $p >> a$ gives

$$A_z \sim -\frac{\mu_0 I}{2\pi}\ln\left(ap^2\right)+A_0$$

Setting this equal to zero (and using the symmetry of the wires for zero net flux between wires) determines A_0,

$$A_0 = \frac{\mu_0 I}{2\pi}\ln\left(ap^2\right) = \frac{\mu_0 I_{tot}}{2\pi}\ln\left(a_{eq}\right)$$

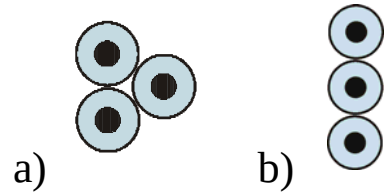

Figure 10. A 3-wire bundle arranged a). in a triangular configuration or b). axially in a cylindrical configuration.

where $3I = I_{tot}$. For large values of $\rho = \sqrt{x^2 + y^2}$ we find the expected form

$$A_z \sim -\frac{\mu_0 I_{tot}}{2\pi} \ln\left(\rho / a_{eq}\right)$$

where the equivalent radius for a triangular arrangement of the three wires (with $p >> a$) is

$$a_{eq} = \left(p^2 a\right)^{1/3} = \left(4a_i^2 a\right)^{1/3} \tag{26}$$

Here we have taken the insulation diameter to be $2a_i = p$. Thus, for the wire-loop arrangement shown in Fig. 10a, (26) is used for the calculation of the loop inductance in (25). The effect of a 3-turn bundle arranged in a triangular configuration versus a cylindrical configuration is discussed in Section 3.5.3.

3.5.2 Cylindrical Wire Configuration

Alternatively let us take the wires to be located at axial positions z_j (wound along a cylinder as in Fig. 10b) and set

$$k_j = \frac{2\sqrt{\rho u}}{\sqrt{\left(u + \rho\right)^2 + \left(z - z_j\right)^2}}$$

The vector potential is then

$$A_\varphi^{tot} = \frac{\mu_0 I}{2\pi} \sqrt{\frac{u}{\rho}} \sum_{j=1}^{n} k_j \left[\left(\frac{2}{k_j^2} - 1 \right) K\left(k_j\right) - \frac{2}{k_j^2} E\left(k_j\right) \right]$$

Now taking the integration along the three loops at $\rho = u$ and at $z = z_{j'} \pm a$ to find the total flux linking the loops gives

$$\Phi = \mu_0 I u \sum_{j'=1}^{n} \sum_{j=1}^{n} k_{jj'} \left[\left(\frac{2}{k_{jj'}^2} - 1 \right) K\left(k_{jj'}\right) - \frac{2}{k_{jj'}^2} E\left(k_{jj'}\right) \right]$$

where for small spacing compared to the radius u,

$$k_{jj'} = \frac{2u}{\sqrt{\left(2u\right)^2 + \left(z_{j'} \pm a - z_j\right)^2}} \sim 1 - \frac{1}{2}\left(z_{j'} \pm a - z_j\right)^2 / \left(2u\right)^2$$

Here we have used

$$K\left(k\right) \sim \ln\left(4/k'\right) \ , \ k \to 1$$
$$k' = \sqrt{1 - k^2}$$
$$k'_{jj'} \sim \left|z_{j'} \pm a - z_j\right| / \left(2u\right)$$
$$E\left(k\right) \sim 1 \ , \ k \to 1$$

Then

$$\Phi \sim \mu_0 I u \sum_{j'=1}^{n} \sum_{j=1}^{n} \left[\ln\left(\frac{8u}{\left|z_{j'} \pm a - z_j\right|} \right) - 2 \right]$$

Assuming that $z_j - z_{j'}$ for uniform loop spacing is only a function of the difference $j - j'$ we can denote it

by $z_{j-j'} = (j - j')\, p$, where $p = 2a_i$ is the diameter of the insulation. For this case

$$\Phi \sim \mu_0 Iun\left[\ln\left(8u/a\right) - 2\right] + \mu_0 Iu\,(n-1)\left[\ln\left(\frac{8u}{|p \pm a|}\right) - 2\right] + \mu_0 Iu\,(n-1)\left[\ln\left(\frac{8u}{|-p \pm a|}\right) - 2\right]$$
$$+\mu_0 Iu\,(n-2)\left[\ln\left(\frac{8u}{|2p \pm a|}\right) - 2\right] + \mu_0 Iu\,(n-2)\left[\ln\left(\frac{8u}{|-2p \pm a|}\right) - 2\right]$$
$$+ \cdots + \mu_0 Iu\,(n-n+1)\left[\ln\left(\frac{8u}{|(n-1)\,p \pm a|}\right) - 2\right] + \mu_0 Iu\,(n-n+1)\left[\ln\left(\frac{8u}{|-(n-1)\,p \pm a|}\right) - 2\right]$$

Dropping the radius a versus the spacing p and specializing to $n = 3$, we have

$$\Phi \sim \mu_0 Iu3^2\left\{\ln\left(8u/a\right) - 2 + \frac{2}{3}\ln\left(a/p\right) - \frac{2}{9}\ln 2\right\} \tag{27}$$

Recalling that for a 3-turn loop the inductance is given by

$$L_a = \Phi/I = \mu_0 u3^2\left[\ln\left(8u/a_{eq}\right) - 2\right]$$

so we can identify from (27) the equivalent radius as

$$a_{eq} = \left(2^{2/3} a p^2\right)^{1/3} \tag{28}$$

3.5.3 Comparisons of Wire Configurations

Using (26) and (28), with $p \approx 2.67\,(2a)$, we obtain 1.31 μH in the 3-turn triangular configuration and 1.24 μH for the 3-turn cylindrical case. Alternatively, Grover [6] gives the estimate resulting from replacement of a cylindrical winding by a strip as

$$L_a \approx n^2 u\mu_0\left[\ln\left(\frac{8u}{np}\right) - \frac{1}{2}\right]$$

which gives 1.24 μH. Thus all these calculations give similar results; we also note that the loop in the 3-turn experiment appears to be a combination of the triangular and cylindrical cases.

3.6 Transmission Line Loads

Cases where various lengths of transmission line are attached to the receiving loop are now considered and the effects of these types of loop loads on the received power are treated in Section 5.3. These lines can have the form of twin-lead lines, twisted pairs, or shielded pairs.

3.6.1 No Insulation Parameters

We now consider the case where the receiving loop $2u = 3$"(16 gauge) is attached to a twin-lead transmission line without insulation. If we consider a $\ell = 7$" long lead with 16 gauge wire ($2a \approx 0.051$") and a separation of $2h_w = 2.67\,(2a)$ then

$$C_{tw}^{\ell} = \frac{\pi\varepsilon_0\ell}{\text{Arccosh}\left(h_w/a\right)} \sim \frac{\pi\varepsilon_0\ell}{\ln\left(2h_w/a\right)} \approx 2.95 \text{ pF}$$

$$L_{tw}^{\ell} = \frac{\mu_0\ell}{\pi}\text{Arccosh}\left(h_w/a\right) \sim \frac{\mu_0\ell}{\pi}\ln\left(2h_w/a\right) \approx 0.12\ \mu\text{H} \tag{29}$$

These would be combined in series with the loop parameters. Note that if we have a tight (we assume no gap between wire insulations and a low twist rate, where this length is nearly the same as ℓ) twisted pair, instead of a twin line, the effective length is similar

$$\ell' = \frac{\ell}{\ell_p}\sqrt{\ell_p^2 + \left(2\pi h_w\right)^2} \approx 7.4 \text{ in}$$

where $\ell_p \approx 1\text{ft}/10$ is the twist period (this parameter is based on the twisted-pair used in the experiment).

Longer leads are considered in the next subsection.

3.6.2 Insulation Parameters

For a twin line with a cylindrical insulation having permittivity ε_2 surrounding the wires (we assume free space outside the insulation) we have the per-unit length inductance L_{tw} and capacitance C_{tw} of [9]

$$L_{tw} = \frac{\mu_0}{\pi}\text{Arccosh}\left(h_w/a\right)$$

(as for the twin line without insulation (29)) and

$$1/C_{tw} \approx \sqrt{\left(\frac{h_w/h_e}{C_0} + \frac{1}{C_2}\right)^2 - \left(\frac{a_i/h_e}{C_0} + \frac{A_2}{C_2}\right)^2} \tag{30}$$

For (30), we have

$$C_0 = \frac{\pi\varepsilon_0}{\text{Arccosh}\left(h/a_i\right)}$$
$$C_2 = \frac{\pi\varepsilon_2}{\ln\left(a_i/a\right)}$$
$$h_e = \sqrt{h_w^2 - a_i^2}$$

and

$$A_2 = 0.7\left(1 - a/a_i\right)\frac{\varepsilon_2 - \varepsilon_0}{\varepsilon_2 + \varepsilon_0}\left(1 - h_e/h_w\right)$$

Note that if $h = a_i$ this reduces to $h_e = 0$ and

$$C_{tw} \approx C_2/\sqrt{\left(1 - A_2\right)\left\{1 + A_2 + 2C_2/\left(\pi\varepsilon_0\right)\right\}}$$

The perfectly-conducting current density on a wire surface (with a return at $2h_w$ away) is

$$K_z^p = \frac{I}{2\pi a}\frac{\sqrt{h_w^2 - a^2}}{h_w + a\sin\varphi}$$

so integration around the perimeter to determine the leading term of the internal impedance per unit length gives

$$P = \frac{1}{2}\left(\frac{1}{2}Z_i\right)|I|^2 \sim \frac{1}{2}\int_C Z_s\left|K_z^p\right|^2 d\ell = \frac{1}{2}\frac{Z_s}{2\pi a}\left(h_w^2 - a^2\right)|I|^2\frac{1}{2\pi}\int_0^{2\pi}\frac{d\varphi}{\left(h_w + a\sin\varphi\right)^2}$$

The one-half factor (in parentheses times Z_i) is introduced due to symmetry because we are integrating over only one wire, and the surface impedance is

$$Z_s = \left(1 - i\right)R_s$$

where

$$R_s = 1/\left(\sigma\delta\right)$$

and the skin depth is

$$\delta = \sqrt{2/\left(\omega\mu\sigma\right)}$$

Thus we can write this as [1]

$$Z_i = R_i - iX_i \sim \frac{Z_s}{\pi a}\frac{h_w}{\sqrt{h_w^2 - a^2}} \tag{31}$$

where we have used [5]

$$\int_{-\pi/2}^{\pi/2}\frac{d\varphi}{\left(h_w + a\sin\varphi\right)^2} = -\frac{\partial}{\partial h_w}\int_0^{\pi}\frac{d\varphi}{\left(h_w + a\cos\varphi\right)} = -\frac{\partial}{\partial h_w}\frac{\pi}{\sqrt{h_w^2 - a^2}}$$

Now taking the wire-to-wire center spacing as $2h_w = 2a_i$ (required to accommodate the insulation radii around the wire a_i) where $2a_i \approx 2.67\,(2a)$, wire diameter $2a = 0.051"$, and relative permittivity of $\varepsilon_2/\varepsilon_0 = \varepsilon_{r2} \approx 2.5$, we find

$$A_2 \approx 0.1876$$
$$C_2 \approx 70.81 \text{ pF/m}$$
$$C_{tw} \approx 31.35 \text{ pF/m}$$
$$L_{tw} \approx 0.6553\ \mu\text{H/m}$$

Thus, in the case of a line having $\ell \approx 0.5$ m (which, over the frequency range examined below, acts as a lumped load), the low frequency load would be $\ell C_{tw} \approx 15$ pF.

In the case of a shielded pair (with the insulations of the pair touching the exterior cylindrical shield) we would find approximately $C_{sh} \approx 2C_{tw}$ (this assumes the capacitance to the images is the same as wire-to-wire) and $L_{sh} \approx L_{tw}/2$. If it is a shielded twisted pair, with large twist length compared to the radius $2h$ of the shield, then the longer effective length ℓ' of the twisted pair must replace ℓ. From (31) the internal impedance per unit length, using the value for copper $\sigma \approx 5.8 \times 10^7$ S/m and $f = 0.584$ MHz, is

$$L_i = X_i/\omega \approx 0.0289\ \mu\text{H/m}$$

where

$$\delta \approx 0.0034 \text{ in}$$
$$R_s \approx 0.2 \text{ mohm}$$
$$R_i \approx 0.106 \text{ ohm/m}$$

Thus, the total inductance per unit length becomes

$$L_{tw} + L_i \approx 0.684\ \mu\text{H/m}$$

with line quality factor

$$\omega\,(L_{tw} + L_i)\,/R_i \approx 23.68$$

3.6.3 Transmission Line Equations

We next use this twin-line per-unit length characterization (C_{tw}, L_{tw}) to compute the input impedance and propagation constant (both having complex values) of the transmission-line load. The transmission-line equations are

$$\frac{dV}{ds} = -ZI = -\left(R - i\omega L_{tw}\right) I$$

and

$$\frac{dI}{ds} = -YV = -\left(G - i\omega C_{tw}\right) V$$

where, for example, $R = R_i$ and G is due to insulation losses. Eliminating I gives

$$\left(\frac{d^2}{ds^2} + \gamma^2\right) V = 0$$

where

$$\gamma^2 = -YZ = -\left(R - i\omega L_{tw}\right)\left(G - i\omega C_{tw}\right) = \omega^2 L_{tw} C_{tw} \left(1 + i\frac{R}{\omega L_{tw}}\right)\left(1 + i\frac{G}{\omega C_{tw}}\right) \tag{32}$$

3.6.4 Solution For Open-Circuit End

In the case that the transmission-line load to the circular receiver is open-circuited (as in Fig. 11), we have

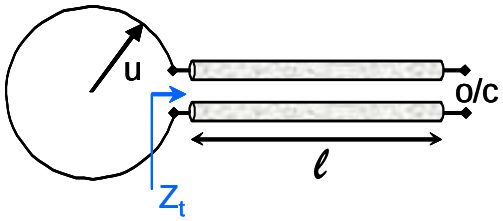

Figure 11. A circular-loop receiver with an open-circuited transmission line load. The radius of the recieving loop is assumed to be $u = 1.5$" throughout this report.

$$I(s=\ell)=0$$
$$V=V_0\cos\gamma(\ell-s)$$

and

$$I=-\frac{1}{Z}\frac{dV}{ds}=-\frac{\gamma}{Z}V_0\sin\gamma(\ell-s)$$

so that the input impedance seen looking into the transmission-line terminals is

$$Z_t=V(0)/I(0)=R_t-iX_t=-\left(\frac{Z}{\gamma}\right)\cot(\gamma\ell)=iZ_0\cot(\gamma\ell)$$

Here the characteristic impedance of the line is

$$Z_0=\sqrt{Z/Y}$$

and from (32)

$$\gamma\approx\omega\sqrt{L_{tw}C_{tw}}\left[1+i/(2Q_t)\right]$$

where

$$1/Q_t\approx\frac{R}{\omega L_{tw}}+\frac{G}{\omega C_{tw}}$$

If we ignore the insulation loss $G\to 0$, we can write

$$Q_t\approx\frac{\omega L_{tw}}{R_i}$$

with

$$R=R_i\approx\frac{R_s}{\pi a}\frac{h_w}{\sqrt{h_w^2-a^2}}$$

and

$$\gamma\ell\approx\omega\sqrt{L_{tw}C_{tw}}\ell\left\{1+i/(2Q_t)\right\} \tag{33}$$

$$Z_0\approx\sqrt{L_{tw}/C_{tw}}\left\{1+i/(2Q_t)\right\} \tag{34}$$
$$Z_t\approx iZ_0\cot(\gamma\ell)$$

Using the above parameters

$$1/\sqrt{L_{tw}C_{tw}}\approx c/1.36$$
$$\sqrt{L_{tw}/C_{tw}}\approx 145\text{ ohms}$$

so that

$$P_{rec}/P_0\sim R_L\frac{\eta_0k_0^2A_r}{(R_L+R_t)^2+(X_t+\omega L_a)^2} \tag{35}$$

Note that this represents the power received by the receiving antenna shown in Fig. 11, normalized by the power generated by the transmitting antenna over the receiving loop area ($P_0=A_rS_0=A_r\frac{1}{2}\eta_0\left|\underline{H}\right|^2$). To define the susceptibility of the receiver, the inverse of this expression will be plotted (Fig. 15) in a subsequent section and compared to the normalized power resulting from alternate receiver configurations.

3.6.5 Solution For Loaded End

If a load is placed at the transmission-line end we have

$$I(s=\ell)=-\frac{1}{Z}\frac{dV}{ds}(s=\ell)=Y_{load}V(s=\ell)$$
$$V=V_0\left[\cos\gamma(\ell-s)+\frac{1}{\gamma}ZY_{load}\sin\gamma(\ell-s)\right]$$

and

$$I=-\frac{1}{Z}\frac{dV}{ds}=V_0\left[-\frac{\gamma}{Z}\sin\gamma(\ell-s)+Y_{load}\cos\gamma(\ell-s)\right]$$

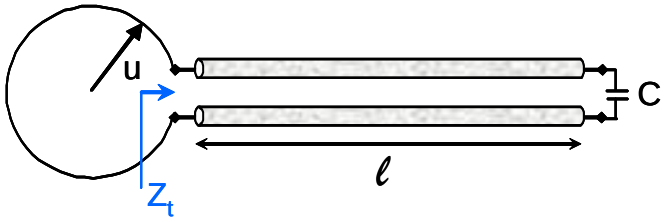

Figure 12. A circular loop receiver connected to a capacitively-loaded transmission line. The radius of the recieving loop is assumed to be $u = 1.5$" throughout this report.

so that

$$Z_t = V(0)/I(0) = \frac{1}{\gamma} Z \frac{\cos(\gamma\ell) + \frac{1}{\gamma} Z Y_{load} \sin(\gamma\ell)}{-\sin(\gamma\ell) + \frac{1}{\gamma} Z Y_{load} \cos(\gamma\ell)}$$
$$= iZ_0 \frac{\cos(\gamma\ell) - iZ_0 Y_{load} \sin(\gamma\ell)}{\sin(\gamma\ell) + iZ_0 Y_{load} \cos(\gamma\ell)} \tag{36}$$

In the case of a capacitively-loaded transmission line as shown in Fig. 12, we have

$$Y_{load} = -i\omega C$$

Calculations for the normalized power received (35) based on the input impedance of a capacitively-loaded transmission line (36) are included in the susceptibility results of Section 5.2.

3.7 Relating Coupled Power to Energy

This section examines the relations between received energy and power, in an effort to simplify the connection in a form that holds in many frequently-encountered situations. For convenience we assume here that free space surrounds the receiver. Let us take the excitation to be a damped sinusoid

$$H_{inc}(t) = H_0 \operatorname{Im}\left[e^{s_0 t}\right] u(t) = H_0 \left(\frac{e^{s_0 t} - e^{s_0^* t}}{2i}\right) u(t) = -H_0 e^{-t/\tau_0} \sin(\omega_0 t)\, u(t)$$

where

$$s_0 = -\omega_0 \left(i + \frac{1}{2Q_0}\right) = -i\omega_0 - 1/\tau_0$$

The transform is defined by

$$H(\omega) = \int_{-\infty}^{\infty} H(t)\, e^{i\omega t} dt$$

so

$$H_{inc}(\omega) = \frac{H_0}{2i} \left(\frac{1}{s_0 + i\omega} - \frac{1}{s_0^* + i\omega}\right)$$

and thus

$$|H_{inc}(\omega)|^2 = H_0^2 \frac{\omega_0}{4\omega} \left[\frac{1}{1/\tau_0^2 + (\omega - \omega_0)^2} - \frac{1}{1/\tau_0^2 + (\omega + \omega_0)^2}\right]$$

Noting from Rayleigh's theorem

$$\int_{-\infty}^{\infty} H^2(t)\, dt = \frac{1}{2\pi} \int_{-\infty}^{\infty} |H(\omega)|^2 d\omega$$

so the received energy can thus be written as

$$W_{rec} = \int_{-\infty}^{\infty} P_{rec}(t)\, dt = \frac{1}{2\pi} \int_{-\infty}^{\infty} A_e(\omega)\, \eta_0 |H_{inc}(\omega)|^2 d\omega$$

3.7.1 Resonance Region

Let us first examine the case where the source carrier frequency ω_0 is near a resonance ω_r of the receiving loop. It is useful to construct an approximate effective area function that obeys the symmetry rule $A_e(-\omega) = A_e(\omega)$ in addition to capturing the low frequency behavior, at least for a resistive load (or a lossy-wire loop). Thus,

$$P_{rec}(\omega) = O\left(\omega^2\right) \frac{1}{2}\eta_0 \left|H_z(0,d)\right|^2$$

so that

$$A_e(\omega) \approx A_e^0 \left[\frac{\omega^2\omega_r^2/Q_r^2}{\left(\omega^2-\omega_r^2\right)^2 + \omega^2\omega_r^2/Q_r^2}\right] = A_e^0 \left[\frac{i\omega/\tau_r}{\omega^2 + i2\omega/\tau_r - \omega_r^2} - \frac{i\omega/\tau_r}{\omega^2 - i2\omega/\tau_r - \omega_r^2}\right] \tag{37}$$

where ω_r is the receive loop resonant frequency, Q_r the resonant quality factor, and the receiving time constant is

$$\omega_r/(2Q_r) = 1/\tau_r$$

Note that this form of the effective area behaves as $O\left(\omega^{-2}\right) = O\left(\lambda^2\right)$ (constant gain) for high frequencies. The poles associated with this effective area can be used to evaluate the energy as

$$W_{rec} \approx -\eta_0 H_0^2 \frac{\omega_0}{2\tau_r} A_e^0 (\tau_0/2) \operatorname{Im}\left[\frac{1}{\left(\omega_0 + i/\tau_0\right)^2 + i2\left(\omega_0 + i/\tau_0\right)/\tau_r - \omega_r^2} - \frac{1}{\left(\omega_0 + i/\tau_0\right)^2 - i2\left(\omega_0 + i/\tau_0\right)/\tau_r - \omega_r^2}\right]$$
$$+\eta_0 H_0^2 \frac{\omega_0}{4\omega_r\tau_r} A_e^0 \operatorname{Re}\left[\frac{1}{1/\tau_0^2 + \left(\omega_r + i/\tau_r - \omega_0\right)^2} - \frac{1}{1/\tau_0^2 + \left(\omega_r + i/\tau_r + \omega_0\right)^2}\right] \tag{38}$$

where τ_0 is the transmitter time constant.

Setting $\omega_0 = \omega_r$ and assuming that $\omega_r\tau_r >> 1$ and $\omega_0\tau_0 >> 1$ gives

$$W_{rec} \approx (\tau_0/2) P_{CW} \left(\frac{\tau_0}{\tau_0 + \tau_r}\right) = (\tau_0/2) P_{CW} \frac{\omega_0\tau_0/(2Q_r)}{\omega_0\tau_0/(2Q_r) + 1} \tag{39}$$

where the continuous-wave average received power is

$$P_{CW} = \frac{1}{2}\eta_0 H_0^2 A_e^0$$

The decaying exponential modulated pulse has an effective pulse width of $(\tau_0/2)$ and the final factor $\tau_0/(\tau_0 + \tau_r)$ reduces the energy further if the receiver time constant is comparable (or longer) than the drive duration. We note that in the case of $\tau_0 >> \tau_r$ then

$$W_{rec} \approx (\tau_0/2) P_{CW} \tag{40}$$

This final result can be interpreted as the case where the effective area is nearly constant in frequency because in such a case we can approximate the energy received as the time domain integral (with fixed effective area). That is,

$$W_{rec} \approx \eta_0 A_e^0 \int_0^\infty H_{inc}^2(t)\, dt$$
$$\approx \eta_0 H_0^2 A_e^0 \int_0^\infty e^{-t2/\tau_0} \sin^2(\omega_0 t)\, dt \approx \frac{1}{2}\eta_0 H_0^2 A_e^0 \int_0^\infty e^{-t2/\tau_0} dt$$
$$\approx (\tau_0/2)\frac{1}{2}\eta_0 H_0^2 A_e^0 \approx (\tau_0/2) P_{CW}$$

which also gives physical insight into (39) (the continuous wave power P_{CW} times the effective transmitter pulse width $\tau_0/2$ times a correction factor for smaller pulse widths $\tau_0/(\tau_0 + \tau_r)$).

3.7.2 Low Frequency Region

Let us now examine the case where the source carrier frequency ω_0 is well below the resonance ω_r of

the receiving loop. First consider the limit of (37)

$$A_e(\omega) \sim A_e^0\left(\omega^2/\omega_r^2\right)/Q_r^2\ ,\ \omega << \omega_r$$

and from Section 3.7

$$|H_{inc}(\omega)|^2 = H_0^2\frac{\omega_0}{4\omega}\left[\frac{1}{1/\tau_0^2+(\omega-\omega_0)^2}-\frac{1}{1/\tau_0^2+(\omega+\omega_0)^2}\right]$$

Because the behavior of the source spectrum is $O\left(\omega^{-4}\right)$ for $\omega >> \omega_0$ we can use the preceding asymptotic form of the effective area to calculate the energy received as

$$W_{rec} \sim \frac{\omega_0\eta_0 A_e^0 H_0^2}{8\pi\omega_r^2 Q_r^2}\int_{-\infty}^{\infty}\omega\left[\frac{1}{1/\tau_0^2+(\omega-\omega_0)^2}-\frac{1}{1/\tau_0^2+(\omega+\omega_0)^2}\right]d\omega$$

Residues in the upper half plane yield

$$W_{rec} \sim (\tau_0/2)\frac{1}{2}\eta_0 H_0^2 A_e^0\left(\omega_0^2/\omega_r^2\right)/Q_r^2 = (\tau_0/2)\,P_{CW}$$

where now

$$P_{CW} = \frac{1}{2}\eta_0 H_0^2 A_e(\omega_0)$$

This is the expected result that was used in the low-frequency coupling analysis presented in Section 3.4.

Now let us consider what happens when there is an open-circuited capacitor in the loop. In this case, based on the preceding results for the coupled power, we take

$$A_e(\omega) \sim A_e^1\omega^4\ ,\ \omega << \omega_r$$

but the resulting energy integral does not then converge at infinity. The high-frequency content of the source is created by the discontinuity in slope of the source waveform at $t = 0$

$$\frac{dH_{inc}}{dt}(0) = \omega_0 H_0$$

This can be avoided by designing a waveform free from this discontinuity in derivatives as discussed in the next subsection. Alternatively we can deal with this problem by realizing that in the time domain the ω^2 operator (the square root of the effective area behavior) is a double derivative

$$-\omega^2 \leftrightarrow \frac{d^2}{dt^2}$$

Thus we can write (here we are ignoring the delta functions arising from derivatives of the unit step $u(t)$ at $t = 0$, taking one sided derivatives there to mimic the case where the waveform and its derivatives are really continuous)

$$\frac{d^2}{dt^2}H_{inc}(t) = \left(1/\tau_0^2-\omega_0^2\right)H_0 e^{-t/\tau_0}\sin(\omega_0 t) - 2\left(\omega_0/\tau_0\right)H_0 e^{-t/\tau_0}\cos(\omega_0 t)\ ,\ t > 0$$

and

$$\left[\frac{d^2}{dt^2}H_{inc}(t)\right]^2 = \omega_0^4 H_0^2\left[\left(1-1/\left(\omega_0\tau_0\right)^2\right)\sin(\omega_0 t)+\frac{2}{\omega_0\tau_0}\cos(\omega_0 t)\right]^2 e^{-2t/\tau_0}\ ,\ t > 0$$

Therefore

$$W_{rec} \sim \int_0^{\infty} A_e^1\eta_0\left[\frac{d^2}{dt^2}H_{inc}(t)\right]^2 dt$$

$$\sim A_e^1\omega_0^4\frac{1}{2}\eta_0 H_0^2\int_0^{\infty} e^{-2t/\tau_0}$$

$$\left[\left(1+1/\left(\omega_0\tau_0\right)^2\right)^2-\left(1-6/\left(\omega_0\tau_0\right)^2+1/\left(\omega_0\tau_0\right)^4\right)\cos(2\omega_0 t)+\frac{4}{\omega_0\tau_0}\left(1-1/\left(\omega_0\tau_0\right)^2\right)\sin(2\omega_0 t)\right]dt$$

or

$$W_{rec} \sim (\tau_0/2)\, A_e(\omega_0)\, \frac{1}{2}\eta_0 H_0^2 \left[\left(1 + 1/(\omega_0\tau_0)^2\right)^2 + \frac{4 - \left(1 - 1/(\omega_0\tau_0)^2\right)^2}{1 + \omega_0^2\tau_0^2} \right]$$

If we assume that $\omega_0\tau_0 >> 1$, then once again we arrive at

$$W_{rec} \sim (\tau_0/2)\, A_e(\omega_0)\, \frac{1}{2}\eta_0 H_0^2 = (\tau_0/2)\, P_{CW} \tag{41}$$

3.7.3 Continuous Source Description

An alternative description of the source in which all time derivatives remain continuous is

$$H_{inc}(t) = H(t)\sin(\omega_0 t)$$

$$H(t) = H_0 \frac{de^{\alpha t}}{1 + e^{\beta(t - t_p)}}$$

This is used to avoid the high-frequency behavior caused by the discontinuity of derivatives at $t = 0$. The inverse double exponential waveform, where the parameters H_0, d, α, and β are adjusted to yield the appropriate rise and fall times of the wave, is often used to describe the EMP waveform (and is in fact often adopted as the requirement). The time interval over which this wave exists, from an analytic point of view, is $-\infty < t < \infty$. From a practical point of view t_p is chosen so that at time $t = 0$ the value of $H(t)$ is vanishingly small, and it can thus be ignored for $t < 0$. The time of peak of $H(t)$ is $t_{pk} = t_p + \frac{1}{\beta}\ln\left(\frac{\alpha}{\beta - \alpha}\right)$. Thus if H_0 is set to the desired peak amplitude, then the constant d is given by

$$d = \beta(\beta - \alpha)^{\alpha/\beta - 1}\alpha^{-\alpha/\beta}\, e^{-\alpha t_p}$$

We should adjust the parameters so that the rise time is consistent with the ω_0 frequency behavior and the fall time is consistent with τ_0. Notice that the factor $e^{-\alpha t_p}$ is typically taken to be vanishingly small. Note that it is possible for the switching operation in the source to introduce some high frequency components (or near discontinuities at $t = 0$) that could contribute to the coupling in the capacitive load case, which would be in addition to the coupling caused by this smooth waveform. The transform of the exponential part is

$$H(\omega) = \int_{-\infty}^{\infty} H(t) e^{i\omega t} dt$$

or

$$H(\omega) = H_0 d \frac{\pi}{\beta} \frac{e^{(\alpha + i\omega)t_p}}{\sin[(\alpha + i\omega)\frac{\pi}{\beta}]}$$

Noting that

$$F(\omega) = \int_{-\infty}^{\infty} \sin(\omega_0 t)\, e^{i\omega t} dt = \frac{1}{2i} \lim_{R\to\infty} \int_{-R}^{R} \left[e^{i(\omega + \omega_0)t} - e^{i(\omega - \omega_0)t} \right] dt$$

$$= i \lim_{R\to\infty} \left[\frac{\sin(\omega - \omega_0)R}{\omega - \omega_0} - \frac{\sin(\omega + \omega_0)R}{\omega + \omega_0} \right] = i\pi \left[\delta(\omega - \omega_0) - \delta(\omega + \omega_0) \right]$$

$$\lim_{R\to\infty} \int_{-b}^{b} f(x) \frac{\sin(xR)}{x} dx = \lim_{R\to\infty} \int_{-bR}^{bR} f(x/R) \frac{\sin(x)}{x} dx = f(0) \lim_{R\to\infty} \left[2\,\mathrm{Si}(bR) \right] = \pi f(0)$$

we can write the transform of the modulated source field as

$$H_{inc}(\omega) = \frac{1}{2\pi} \int_{-\infty}^{\infty} H(\omega') F(\omega - \omega')\, d\omega' = \frac{i}{2} \int_{-\infty}^{\infty} H(\omega') \left[\delta(\omega - \omega_0 - \omega') - \delta(\omega + \omega_0 - \omega') \right] d\omega'$$

$$= \frac{i}{2} \left[H(\omega - \omega_0) - H(\omega + \omega_0) \right] = \frac{i}{2} H_0 d \frac{\pi}{\beta} \left\{ \frac{e^{(\alpha + i(\omega - \omega_0))t_p}}{\sin[(\alpha + i(\omega - \omega_0))\pi/\beta]} - \frac{e^{(\alpha + i(\omega + \omega_0))t_p}}{\sin[(\alpha + i(\omega + \omega_0))\pi/\beta]} \right\}$$

This can then in principle be integrated to yield the energy

$$W_{rec} = \int_{-\infty}^{\infty} P_{rec}(t)\, dt = \frac{1}{2\pi} \int_{-\infty}^{\infty} A_e(\omega)\, \eta_0\, |H_{inc}(\omega)|^2\, d\omega$$

4 RESULTS

We now illustrate coupling results for various transmit-receive scenarios. In this section we assume free space surrounding the loop.

4.1 Rectangular Transmitting Loop And Circular Receiving Loop

If we consider the magnetic field generated by a rectangular loop as used in the test (as discussed in Section 2.2), S_0 becomes

$$S_0 = \left(3.8 \text{ W}/(\text{A} - \text{m})^2\right) I^2$$

where from (6) and (3)

$$q_m \approx \left(3.7 \times 10^{-7} \text{ H/m}\right) I$$
$$H_x = (0.14/\text{m})\, I$$

at $x \approx 6.5$" (measured from the center of the plates and with $d = 5$"), $y = 0$, and absolute position $z = 0$ (2Δ is near the average value $\left(\frac{1.75+1.0}{2}\right)$" and $2h \approx 11.5$"). The geometry of the transmitter is shown in Fig. 1. The power received in this case (with the axes of the two loops aligned) becomes

$$P_r^{rect} = I^2 \left(2.9 \times 10^{-6} \text{ W/A}^2\right)$$

Using the source parameters of $I = 140\ kA$ and $\tau_0 = 7\ \mu s$, this gives an energy received at 0.584 MHz of

$$W_r^{rect} = 200 \text{ mJ}$$

(40). Note that going from a transmitting circular loop of $b = 2.5$" to a transmitting rectangular loop with the dimensions listed above, there is a drop of about a factor of 25 in the energy received (see Table 3). Moving the receive location up towards the bend in the transmitting loop to $z = 4$"(this corresponds to the test position of 9.5" from the base of the primary, where now 2Δ approaches the top value), W_r^{rect} decreases to 96 mJ. Decreasing the transmit/receive separation to $d = 3$" with $z = 4$", there is significant increase in the received energy with the result going to 586 mJ from the previous value of 96 mJ. A summary of the received energies based on a circular receiving loop and a rectangular loop transmitter separated by $d = 5$" for absolute positions $z = 0$ and $z = 4$"are given in Tables 4 and 5.

Table 4. Energy received using a circular loop receiver of u=1.5" and a rectangular loop transmitter as shown in Fig. 1. A transmit/receive seperation of d=5" is assumed at z=0".

f [MHz]	W_{rec} [mJ]
0.584	200
1	351
10	572
60	575

The variation in the received power versus the separation between the transmit (rectangular) and receive (circular) loops is shown in Figure 13. (Note that $z = 0$ corresponds to the center of the primary loop and the distance $z = 4$" corresponds to the test position up towards the bend of the transmitting rectangular loop (Fig. 1). For convenience, the received energy has been normalized by the square of the peak drive current I^2 (a time constant of $\tau_0 = 7\ \mu s$ is assumed).

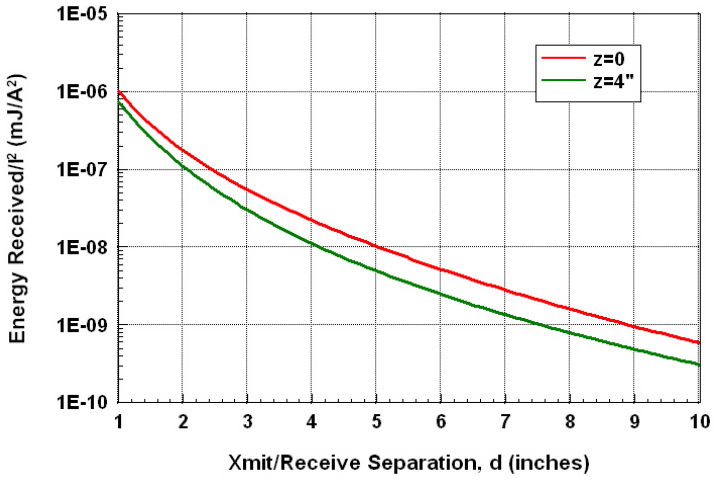

Figure 13. The normalized received energy versus the spacing d between the edge of the transmitting rectangular loop and the center of the receiver (single turn). The case $z = 0$ corresponds to the two axes of the loops aligning, whereas $z = 4$" corresponds to a displacement of the receive center from the transmitting loop center (Fig. 1).

Table 5. Energy received using a circular loop receiver of u=1.5" and a rectangular loop transmitter as shown in Fig. 1. A transmit/receive seperation of d=5" is assumed at z=4".

f [MHz]	W_{rec} [mJ]
0.584	96
1	169
10	275
60	277

It is important to note that values of received energy shown in Fig. 13 have been obtained by sampling the transmitting field (associated with the rectangular loop for this case) at a single point (center) through the receiving loop. This was done for convenience and the agreement between this and an integration over the receiving loop was found to be reasonably accurate. This comparison, in the form of a graph, was presented in Fig. 9 (dashed green curve versus solid orange curve).

A comparison between the center-point and integrated received energy calculations is also provided in Table 6 for a drive current of $I = 140$ kA and an absolute location of $z = 5.5$" (relative location in symmetric system of 5.25"). Here the table columns for the first four rows represent the distance d from the edge of the transmit loop, the analytic constant magnetic charge density result using a center point value of the magnetic field, the analytic result using an integration of the magnetic field over the loop, and the analytic result using an integration (including the loop alone 0.199 μH$\rightarrow -i0.730$ ohms, and the theoretical result for a lead inductance of 7.4" length in the loop circuit 0.327 μH$\rightarrow -i1.20$ ohms), respectively. The second set of four rows in this table give the analytic results using the mutual inductance from the linear approximation for the magnetic charge density. The third set of four rows uses the magnetic vector potential results for the mutual inductance. The last two rows in this table used the mutual inductance from the EIGER simulation instead of the analytic formulas. Notice that these results are all relatively close to each other (for the same value of d and load); the analytic results for $d = 3$" using the magnetic vector potential model are quite close to the EIGER results.

4.2 Rectangular Transmitting Loop And Three Turn Circular Receiving Loop

If we now consider the same rectangular transmitting loop with a 3-turn circular receiver (of 3" diameter), the received power is

$$P_{rec}^{n\ turns} = \frac{1}{2} R_L \frac{|nV_{oc}|^2}{\left|n^2 Z_a^{(n)} + Z_L\right|^2} = \frac{1}{2} R_L \frac{\eta_0 \left(nk_0 A_r\right)^2}{\left|n^2 Z_a^{(n)} + Z_L\right|^2} \eta_0 \left|H_z\left(0,d\right)\right|^2$$

and the calculated received energies are tabulated in Table 7. (For the purposes of creating Table 7 the self-inductance of the 3-turn receiver is taken to be 1.31μH.) Comparing the analytic value of 55.1 mJ at $d = 5$" from Table 7 to the single-turn result of 96 mJ in Table 5, it is clear that the energy received by the transmitter is decreased with the additional loop turns (for this low impedance load of $Z_L = 1\ \Omega$).

5 SUSCEPTIBILITY CURVES

This section will quantitatively examine the major factors involved in loop coupling in the simplest possible way. From above (Section 3.1) we can write the received power in terms of the external magnetic

Table 6. Energy received using a 1-turn circular loop receiver of u=1.5" and a rectangular loop transmitter as shown in Fig. 1. In the analysis, a position of z=5.5" and a transmit frequency of 0.584 MHz are assumed, with a peak current of 140 kA and an exponential decay time of 7 microseconds.

d	W_{rec}: Center Point	W_{rec}: Integrated Flux	W_{rec}: Integrated Flux & Inductance
3 in	251 mJ	199 mJ	125 mJ
5 in	46.5 mJ	42.3 mJ	26.6 mJ
7 in	14.3 mJ	13.6 mJ	8.6 mJ
d	W_{rec}^{Lin}: Center Point	W_{rec}^{Lin}: Integrated Flux	W_{rec}^{Lin}: Integrated Flux & Inductance
3 in	269 mJ	216 mJ	135 mJ
5 in	53.5 mJ	49.0 mJ	30.8 mJ
7 in	17.5 mJ	16.7 mJ	10.5 mJ
d	W_{rec}^{Vect}: Center Point	W_{rec}^{Vect}: Integrated Flux	W_{rec}^{Vect}: Integrated Flux & Inductance
3 in	520 mJ	416 mJ	261 mJ
5 in	98.3 mJ	89.6 mJ	56.3 mJ
7 in	30.5 mJ	29.0 mJ	18.2 mJ
d	W_{rec}^{EIG}: Center Point	W_{rec}^{EIG}: Integrated Flux	W_{rec}^{EIG}: Integrated Flux & Inductance
3 in	516 mJ	421 mJ	264 mJ

field at the loop as

$$P_{rec} = \frac{1}{2} R_L \frac{|V_{oc}|^2}{|Z_a + Z_L|^2} \sim R_L \frac{\eta_0 \left(k_0 A_r\right)^2}{|Z_a + Z_L|^2} \frac{1}{2} \eta_0 |H_z|^2 \tag{42}$$

where A_r is the loop area which for the circle is πu^2, Z_a is the loop impedance and Z_L is the load impedance. We again assume in this section that we are well below the loop resonant frequency (and thus we are ignoring the radiation resistance and the intrinsic capacitance) and therefore take

$$Z_a \sim -i\omega L_a$$

$$L_a \sim u\mu_0 \left[\ln\left(8u/a\right) - 2\right] \approx 0.199 \ \mu\text{H}$$

We again take $R_L = 1\ \Omega$, but consider several additional loads to generate a total complex impedance of Z_L.

As before, the energy and power are taken to be connected through

$$W_{rec} \approx \left(\tau_0/2\right) P_{rec}$$

(41). But note that if the load thermal time constant is longer than the preceding microsecond electrical pulse width τ_0, we can, in principle, lengthen the driven pulse to match this thermal time constant and then drop the power requirements (and required power density) to achieve the same coupled energy.

5.0.1 Resistive Load

In the first case we again take

$$Z_L = R_L = 1\ \Omega$$

Then the received power (42) can be written as

$$P_{rec}/P_0 \sim R_L \frac{\eta_0 \left(k_0^2 A_r\right)}{R_L^2 + \omega^2 L_a^2} \tag{43}$$

where the power from the transmitter produced over the received loop is

$$P_0 = A_r S_0$$

Table 7. Energy received using a 3-turn circular loop receiver of u=1.5" and a rectangular loop transmitter as shown in Fig. 1. A position of z=4" and a transmit frequency of 0.584 MHz are assumed.

d [in.]	W_{rec} [mJ]: Analy.
3	335
5	55.1
7	15.2

with

$$S_0 = \frac{1}{2}\eta_0 \left|H_z\right|^2$$

The behavior of (43) in frequency changes from $O\left(\omega^2\right)$ for the low frequencies to a constant near

$$1 = \omega_0 L_a / R_L \approx \omega_0 \left(0.199\ \mu\text{s}\right)$$

or $\omega_0 = 2\pi f_0$ with $f_0 \approx 0.8$ MHz. Thus, for the case of a resistive load (and in the limit of low frequencies) we have

$$P_{rec}/P_0 \sim \frac{\eta_0 k_0^2 A_r}{R_L} \approx \left(7.552 \times 10^{-4}\right) f^2\,(\text{MHz}) \tag{44}$$

and as the frequency increases beyond $f_0 \approx 0.8$ MHz, the normalized power received becomes

$$P_{rec}/P_0 \sim \frac{\eta_0 \left(A_r/c^2\right)/R_L}{\left(L_a/R_L\right)^2} \approx 4.833 \times 10^{-4} \tag{45}$$

(For obtaining these expressions, a loop of $2u = 3$" has been assumed.) Note that based on these two limiting cases in frequencies, the behavior of the received power is as shown in Fig. 14 (where the region about $f_0 \approx 0.8$ MHz has been approximated by the asymptote curves).

5.1 Capacitive and Resistive Load

Another case we can take is

$$Z_L = R_L + Z_t$$

where Z_t is an extra complex load impedance associated with an open circuit capacitance C_t

$$Z_t = 1/\left(-i\omega C_t\right)$$

In this situation (where the load is a pure capacitance) we assume that this capacitive reactance dominates over the load resistance and antenna inductance so that from (42)

$$P_{rec}/P_0 \sim R_L \eta_0 \left(k_0 \omega C_t\right)^2 A_r$$

The behavior here is $O\left(\omega^4\right)$ in frequency and $O\left(C_t^2\right)$ in the capacitance. For the case where

$$C_t = C_a \approx \frac{\pi^2 \varepsilon_o u/3}{\ln\left(u/a\right)} \approx 0.272\ \text{pF}$$

we obtain

$$P_{rec}/P_0 \approx \left(2.206 \times 10^{-15}\right) f^4\,(\text{MHz})$$

As a second example, the load capacitance to the circular loop is increased to

$$C_t \approx 15\ \text{pF}$$

(as for a short section of open-circuited transmission line, discussed above) and this yields

$$P_{rec}/P_0 \approx \left(6.71 \times 10^{-12}\right) f^4\,(\text{MHz})$$

The results for the capacitively-loaded circular loops are included in Fig. 14, where it is clear that the

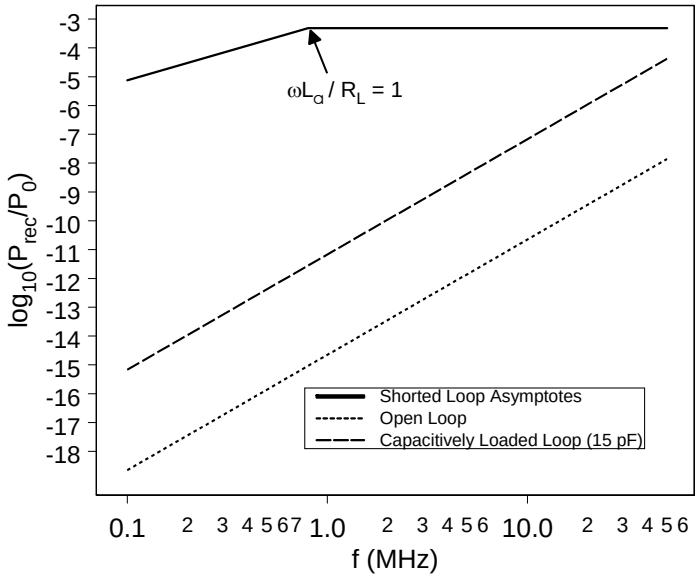

Figure 14. Received power to transmit power ratio for various receiving antenna configurations. All curves assume a 1.5" radius circular loop receiver with a resistive 1 Ω load.

received power decreases dramatically when the circular loop is anything but short-circuited.

We can also fix the energy threshold and optimize the pulse width to the thermal time constant, thereby giving the required power density produced by the transmitter over the receiving loop as a function of frequency. In this case we instead plot the inverted ratio P_0/P_{rec} (or S_0/P_{rec}) as shown below.

5.2 Transmission-Line Load

While thus far results corresponding to discrete loads to the circular-loop receiver have been considered, in this section we examine the case where a longer transmission line is attached to the receiving loop. We consider a transmission line characterized with the parameters

$$C_{tw} \approx 31.35 \text{ pF/m}$$

$$L_{tw} \approx 0.6553 \ \mu\text{H/m}$$

$$R_i \sim \frac{R_s}{\pi a} \frac{h_w}{\sqrt{h_w^2 - a^2}} \approx 0.106 \text{ ohm/m}$$

(Section 3.6.2) which then yields

$$\sqrt{L_{tw}/C_{tw}} \approx 145 \text{ ohms}$$

$$Q_t \approx \omega \left(6.18 \times 10^{-6}\right)$$

$$\sqrt{L_{tw} C_{tw}} \approx 1.36/c$$

At this point the propagation constant γ and characteristic impedance Z_0 of the transmission line can be calculated ((33) and (34)) to ultimately arrive at the input impedance $Z_t = R_t - iX_t$ seen looking down the transmission line (as shown in Figs. 11 and 12). In Fig. 15, results based on the normalized received power (determined from (35)) are given for various length transmission lines (all terminated in an open circuit). For comparison, results for a short-circuited circular loop, an open loop, and a capacitively-loaded circular loop are also provided (all with $R_L = 1$ Ω). Figure 15 demonstrates that coupling is facilitated as

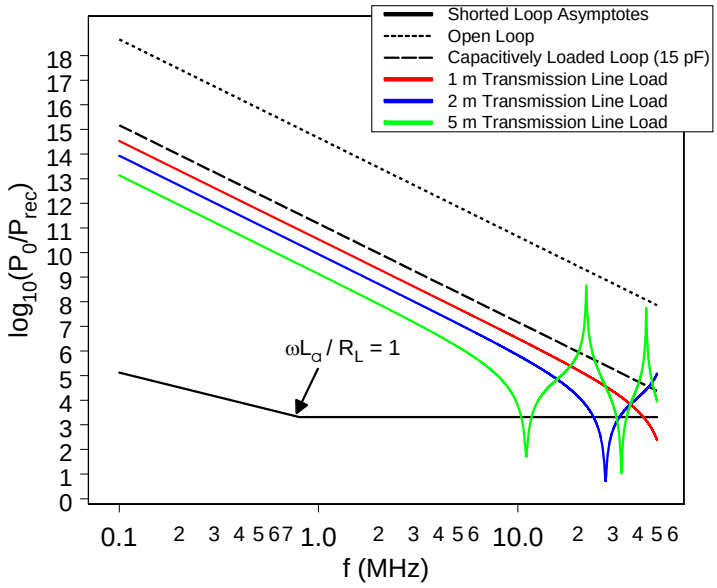

Figure 15. Transmitting power to receive power ratio for various receiving antenna configurations, including open-circuited transmission lines attached to the receiving loop. All curves assume a 1.5" radius circular loop receiver with a resistive 1 Ω load.

transmission-line sections are introduced to the receiving antenna (in this case a 1.5" radius circular loop has been assumed) and the frequency is increased.

For convenience, the data in Fig. 15 has been renormalized by the area of the receiving loop ($A_r = \pi u^2$) so that the ordinate axis becomes S_0/P_{rec} in units of inverse square meters, as given in Fig. 16.

While Figs. 15 and 16 include results for open-circuited transmission lines, Fig. 17 shows the effect of a load at the end of the transmission line (in this case the same capacitive load we discussed previously, simulating a short section of another line). These calculations are based on the analysis presented in Section 3.6.5 and can be compared to the unterminated transmission line results given above. A 15 pF capacitor is considered (Fig. 12).

It is interesting to note that if we instead move the capacitive load from the end of the line to the beginning of the line (in series with the transmission line and again with a value of 15 pF), the resonant responses of the transmission lines are pushed out to slightly higher frequencies and the minimums of P_0/P_{rec} do not go quite as low (at least in the frequency range we are considering). This particular receiving antenna configuration is shown in Fig. 18 and the corresponding behavior is included in Fig. 19. For this case,

$$Z_t = \frac{i}{\omega C_{load}} + iZ_0 \cot(\gamma \ell)$$

5.3 Antenna-Transmission Line Mode

In the previous results the drive was limited to the loop alone and the attached cables acted as loads.

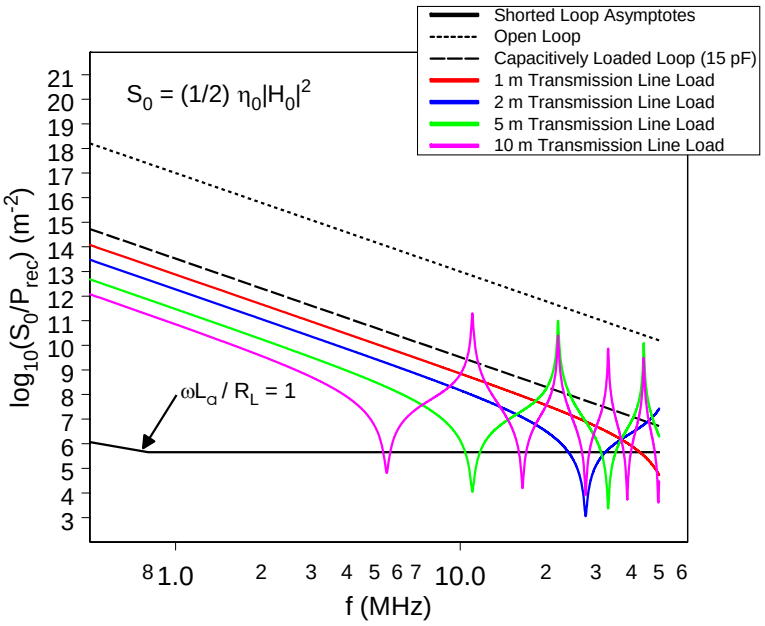

Figure 16. Transmitting power density (S_0) to receive power ratio for various receiving antenna configurations, including open-circuited transmission lines attached to the receiving loop. All curves assume a 1.5" radius circular loop receiver with a resistive 1 Ω load and a rectangular loop transmitter as shown in Fig. 1.

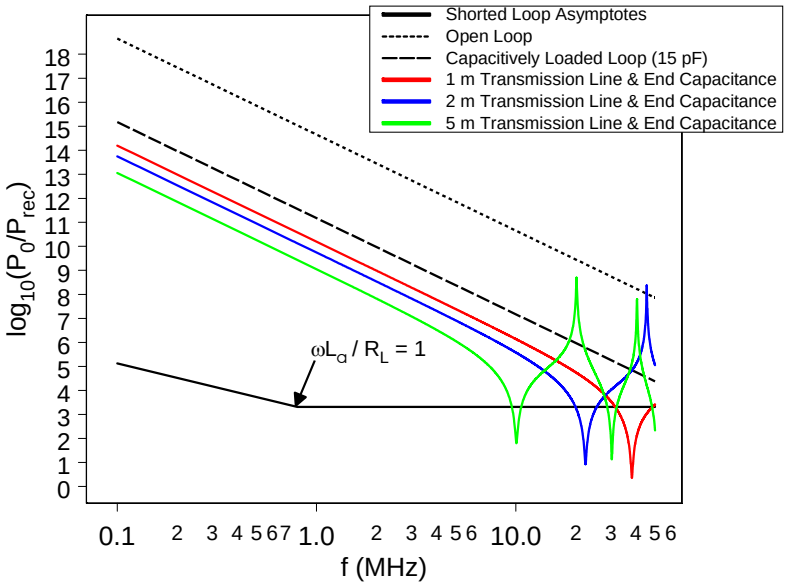

Figure 17. Transmitting power to receive power ratio for various receiving antenna configurations, including capacitively-loaded transmission lines attached to the receiving loop. All curves assume a 1.5" radius circular loop receiver with a resistive 1 Ω load.

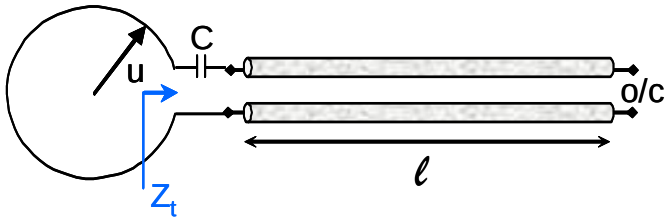

Figure 18. A circular loop receiver connected to a capacitor in series with an open-circuited transmission line. The radius of the recieving loop is assumed to be $u = 1.5$" throughout this report.

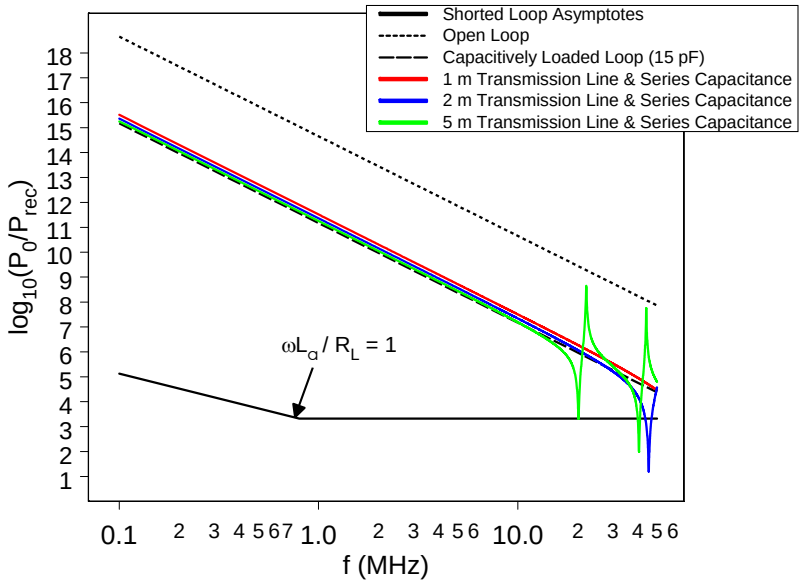

Figure 19. Transmitting power to receive power ratio for various receiving antenna configurations, including a series capacitor and transmission line attached to the received loop. All curves assume a 1.5" radius circular loop receiver with a resistive 1 Ω load.

Figure 20. A twisted pair cable with a low impedance load in one wire.

Now we consider the case where the drive is to the bulk current of the cable and part of this current drives the load. Figure 20 shows the topology. This cable can be in free space or above a perfect ground plane.

The two wires in the transmission line act together in free space as an antenna, or together in concert with the ground plane as a bulk transmission line. For simplicity in this section we assume that the load is placed at the center of the cable (in this special case the even resonances with $kh = (m - 1/2)\,\pi$ will be present but the odd resonances $kh = m\pi$ will not be excited, where $2h = \ell$ is the cable length).

5.3.1 Common And Differential Decompositions

The bulk current can be decomposed in general into a sum of common mode (equal currents) and differential mode (oppositely directed currents). In the case of symmetric wires this is the natural decomposition. On the other hand with asymmetrical wires it is more natural to split the bulk current into an antenna mode (with no potential difference between wires) and a type of differential mode (with a voltage differential between wires). For the remainder of this section we assume symmetric wire cross sections.

Let us consider symmetric wires and write the common and differential mode currents and voltages in terms of the wire currents $I_\pm$ and $V_\pm$ as

$$\begin{aligned} I_c &= I_+ + I_- \\ I_d &= I_+ - I_- \\ V_c &= V_+ + V_- \\ V_d &= V_+ - V_- \end{aligned}$$

We will model both the bulk current (antenna mode or transmission line mode) and the differential mode current in terms of transmission line models.

5.3.2 Antenna Problem

In the case of an antenna excited by the axial electric field along the wires we write

$$\begin{aligned} \frac{dV_c}{dz} &= -Z_c I_c + E_z^{inc} \\ \frac{dI_c}{dz} &= -Y_c V_c \end{aligned} \tag{46}$$

where Z_c and Y_c are "average" (we assume the wires are thin compared to the line length) impedance per unit length and admittance per unit length parameters along the antenna. These can be written using duality [10] as

$$\begin{aligned} Z_c &= \Delta Z_L - i\omega L^{pe} \\ L^{pe} &\approx \mu_0 \Omega_e / (2\pi) \\ 1/Y_c &= \Delta Z_C + \frac{1}{-i\omega C^{pe}} \\ C^{pe} &\approx 2\pi\varepsilon_0 / \Omega_e \end{aligned}$$

where the expansion parameter in thin antenna theory is taken as

$$\Omega_e = \Omega + C_e$$

(the choice of the constant C_e can be made to achieve first order accuracy in the quasistatic solution of the

antenna) and the fatness parameter is

$$\Omega = 2\ln(2h/a_{eq})$$

where the transmission line length is

$$2h = \ell$$

For a scattering antenna $C_e = 2(\ln 2 - 7/3)$ [10] and for a center load $C_e = -2(1+\ln 2)$. Note that these two choices are nearly consistent (if we approximate $\ln 2 \approx 0.693 \approx 2/3$ then from both we find $C_e \approx -10/3$). The parameter a_{eq} is the equivalent radius of the two wires operating in a common mode. Let us again take twin 16 gauge wires ($2a \approx 0.051$") and a separation of $2h_w = 2.67\,(2a)$

$$a_{eq} = \sqrt{ah_w} \approx 0.04167 \text{ in}$$

The parameters ΔZ_L and ΔZ_C can account for dielectric media surrounding the wires. For example in the case of a single wire of radius a with insulation ε_i of radius a_i, we can take $a_{eq} = a_i$, $\Delta Z_L = (1-i)\,R_s/(2\pi a) - i\omega(\mu_0/\pi)\ln(a_i/a)$, $1/\Delta Z_C = -i\omega(\pi\varepsilon_i)/\ln(a_i/a)$. In our case for the twin wire line we use the radius a_{eq} but include the wire losses (inserting one half for two parallel wires sharing the common mode current)

$$\Delta Z_L = \frac{1}{2}(1-i)\,R_s/(2\pi a)$$

and we ignore the correction to the capacitance per unit length of the common mode due to the insulation

$$\Delta Z_C \approx 0$$

We can account for radiation and higher-order reactive terms by modifying (46) to

$$\frac{dV_c}{dz} = -(Z_c + Z_{rad})\,I_c + E_z^{inc}$$

and eliminating the voltage gives

$$\left(\frac{d^2}{dz^2} + k^2\right) I_c = -Y_c E_z^{inc}$$

where the propagation constant is (not to be confused with the argument of the elliptic integrals in the beginning of the report)

$$k = \sqrt{-(Z_c + Z_{rad})\,Y_c}$$

where for $k \approx k_0$ (and based on a current distribution proportional to $\cos k_0 z - \cos k_0 h$) [10]

$$Z_{rad} = R_{rad} - iX_{rad}$$

$$R_{rad} = \eta_0 \frac{\mathrm{Cin}(4k_0h) + 4\,\mathrm{Si}(2k_0h)\cos k_0h\,(k_0h\cos k_0h - \sin k_0h) - \sin^2(2k_0h)}{2\pi h\,[1 + \cos k_0h\,(2\cos k_0h - 3\sin k_0h/(k_0h))]}$$

$$X_{rad} = \eta_0 \frac{4\cos k_0h\,(k_0h\cos k_0h - \sin k_0h)\,\{\ln 2 - C_e/2 - \mathrm{Cin}(2k_0h)\} + \mathrm{Si}(4k_0h) - 2\cos^2 k_0h\sin(2k_0h)}{2\pi h\,[1 + \cos k_0h\,(2\cos k_0h - 3\sin k_0h/(k_0h))]}$$

where the sine and cosine integrals are ($\gamma' \approx 0.5772156649$ is Euler's constant)

$$\mathrm{Cin}(x) = \int_0^x \frac{1-\cos u}{u}du = -\,\mathrm{Ci}(x) + \ln x + \gamma'$$

$$\mathrm{Si}(x) = \int_0^x \frac{\sin u}{u}du$$

$$\mathrm{Ci}(x) = \int_x^\infty \frac{\cos u}{u}du$$

The current at the ends of the antenna vanishes

$$I_c(\pm h) = 0$$

We assume that the incident plane wave has axial field

$$E_z^{inc} = E_{0z}e^{ik_0z\cos\theta_0}$$

and then the common-mode antenna current has the form

$$I_c = A\sin kz + B\cos kz - Y_c E_{0z} e^{ik_0 z\cos\theta_0} / \left(k^2 - k_0^2\cos^2\theta_0\right)$$

For normal incidence (with respect to the z axis) $\theta_0 = \pi/2$ we make this even with respect to $z = 0$

$$I_c = \left(\cos kz - \cos kh\right) Y_c E_{0z} / \left(k^2\cos kh\right) + A\sin k\left(h - |z|\right)$$

Note that the final term has a different distribution than that assumed for the Y_{rad} calculation, $\cos kz - \cos kh$. However near resonance $kh = (m - 1/2)\,\pi$ where these terms have their largest impact on the mode amplitude, we have $\cos kh = 0$ and $\sin k\left(h - |z|\right) = (-1)^{m-1}\cos kz$.

Next, the differential mode satisfies the transmission line equations

$$\frac{dV_d}{dz} = -Z_d I_d$$

$$\frac{dI_d}{dz} = -Y_d V_d$$

where we have assumed that the wires are twisted and have ignored any distributed source terms in the differential mode (it will be driven by the load alone). The formulas for the impedance and admittance per unit length of the differential mode with twisted insulated wires can be found back in the previous section on insulated wires.

$$Y_d \approx -i\omega C_{tw}$$

$$C_{tw} \approx 31.35 \text{ pF/m}$$

$$Z_d \approx Z_i - i\omega L_{tw}$$

$$L_{tw} \approx 0.6553 \ \mu\text{H/m}$$

$$Z_i = (1 - i)\,R_i$$

$$R_i = \frac{R_s}{\pi a}\frac{h_w}{\sqrt{h_w^2 - a^2}} \approx 0.106 \text{ ohm/m}$$

We take open circuits at the ends so that

$$I_d\left(\pm h'\right) = 0$$

where the twisted half length is

$$h' = \ell'/2 = h\sqrt{1 + \left(2\pi h_w/\ell_p\right)^2}$$

Again we assume no gap between wire insulations and a low twist rate, where this length h' is nearly the same as h (the use of h' in the differential mode is thought to result in a slight overestimate of the twist effect). This twisting also adds extra impedance per unit length to the common mode which could be accounted for by small additions to ΔZ_L and ΔZ_C, but we neglect it (the use of h in the common mode is thought to result in a slight underestimate of the twist effect). Eliminating the voltage V_d in the transmission line equations gives

$$\left(\frac{d^2}{dz^2} + \gamma^2\right) I_d = 0$$

where the differential propagation constant along the pair is

$$\gamma = \sqrt{-Z_d Y_d}$$

The solution has the form

$$I_d = A_0\sin\gamma z + B_0\cos\gamma z$$

and for normal incidence, the even solution obeying the open-circuit end condition is

$$I_d = A_0\sin\gamma\left(h' - |z|\right)$$

Now if we place a load Z_L at the center of one wire, say the + one, we have

$$V_+(-0) - V_+(+0) = \frac{1}{2}\left[I_+(+0) + I_+(-0)\right] = I_+(0)\,Z_L$$

and

$$I_+(-0) = I_+(+0)$$

$$V_-(-0) = V_-(+0)$$

$$I_-(-0) = I_-(+0)$$

or

$$V_d(-0) - V_d(+0) = \frac{1}{2}\left[I_c(0) + I_d(0)\right] Z_L = V_c(-0) - V_c(+0)$$

$$I_c(-0) = I_c(+0)$$

$$I_d(-0) = I_d(+0)$$

Thus, from the above representations

$$\frac{dI_c}{dz} = -Y_c V_c = -\sin kz Y_c E_{0z} / \left(k^2 \cos kh\right) - kA\cos k\left(h - |z|\right)\operatorname{sgn}(z)$$

$$\frac{dI_d}{dz} = -Y_d V_d = -\gamma A_0 \cos\gamma\left(h' - |z|\right)\operatorname{sgn}(z)$$

and

$$-2\frac{\gamma}{Y_d} A_0 \cos\gamma h' =$$

$$\frac{1}{2}\left[\left(1 - \cos kh\right) Y_c E_{0z} / \left(k^2 \cos kh\right) + A\sin kh + A_0 \sin\gamma h'\right] Z_L$$

$$= -2\frac{k}{Y_c} A\cos kh$$

or

$$\frac{1}{2}\left[\left(1 - \cos kh\right) Y_c E_{0z} / \left(k^2 \cos kh\right) + A_0 \sin\gamma h'\right] Z_L = -A\left(\frac{1}{2} Z_L \sin kh + 2\frac{k}{Y_c}\cos kh\right)$$

$$\frac{1}{2}\left[\left(1 - \cos kh\right) Y_c E_{0z} / \left(k^2 \cos kh\right) + A\sin kh\right] Z_L = -A_0\left(\frac{1}{2} Z_L \sin\gamma h' + 2\frac{\gamma}{Y_d}\cos\gamma h'\right)$$

and

$$-\frac{\frac{1}{2}\left(1 - \cos kh\right) Z_L Y_c E_{0z} / \left(k^2 \cos kh\right)}{\frac{1}{2} Z_L \sin\gamma h' + \left(\frac{\gamma Y_c}{k Y_d}\frac{\cos\gamma h'}{\cos kh}\right)\left(\frac{1}{2} Z_L \sin kh + 2\frac{k}{Y_c}\cos kh\right)} = A_0$$

$$-\frac{\left(\frac{\gamma Y_c}{k Y_d}\frac{\cos\gamma h'}{\cos kh}\right)\frac{1}{2}\left(1 - \cos kh\right) Z_L Y_c E_{0z} / \left(k^2 \cos kh\right)}{\frac{1}{2} Z_L \sin\gamma h' + \left(\frac{\gamma Y_c}{k Y_d}\frac{\cos\gamma h'}{\cos kh}\right)\left(\frac{1}{2} Z_L \sin kh + 2\frac{k}{Y_c}\cos kh\right)} = A$$

Then the current of interest is

$$I_+(0) = \frac{1}{2}\left[I_c(0) + I_d(0)\right] = \frac{1}{2}\left[\left(1 - \cos kh\right) Y_c E_{0z} / \left(k^2 \cos kh\right) + A\sin kh + A_0 \sin\gamma h'\right]$$

$$= \frac{\left(\frac{\gamma Y_c}{k Y_d}\frac{\cos\gamma h'}{\cos kh}\right)\left(1 - \cos kh\right) E_{0z}/k}{\frac{1}{2} Z_L \sin\gamma h' + \left(\frac{\gamma Y_c}{k Y_d}\frac{\cos\gamma h'}{\cos kh}\right)\left(\frac{1}{2} Z_L \sin kh + 2\frac{k}{Y_c}\cos kh\right)}$$

As a check, notice that if $Z_L = 0$ we find that the load current becomes half the common-mode current

$$I_+(0) = \frac{1}{2}\left(1 - \cos kh\right) Y_c E_{0z} / \left(k^2 \cos kh\right) = \frac{1}{2} I_c(0)$$

because $A = 0$ (and $A_0 = 0$) in this limit. This type of result is used below as an approximation to simplify the results for a low impedance load.

Limited Drive Region Suppose that the drive is limited to the region near the cable center with length

$$\ell_0 = 2h_0$$

with constant field E_{0z} in this region and zero drive field outside this region (this crudely simulates the case where the source has limited spatial extent). Then we can write

$$\left(\frac{d^2}{dz^2} + k^2\right) I_c = -Y_c E_{0z} \ , \ 0 < |z| < \ell_0/2 = h_0 \tag{47}$$

$$\left(\frac{d^2}{dz^2} + k^2\right) I_c = 0 \ , \ \ell_0/2 = h_0 < |z| < \ell/2 = h$$

$$I_c = A \sin k\left(h - |z|\right) + B \cos kz - Y_c E_{0z}/k^2 \ , \ 0 < |z| < h_0$$

$$I_c = A_1 \sin k\left(h - |z|\right) \ , \ h_0 < |z| < h$$

Matching the current and its derivative at $z = h_0$, we obtain

$$B \cos kh_0 = (A_1 - A) \sin k\left(h - h_0\right) + Y_c E_{0z}/k^2$$

$$B \sin kh_0 = (A_1 - A) \cos k\left(h - h_0\right)$$

or

$$(A_1 - A) = Y_c E_{0z} \sin kh_0 / \left(k^2 \cos kh\right)$$

$$B = \cos k\left(h - h_0\right) Y_c E_{0z} / \left(k^2 \cos kh\right)$$

and thus

$$I_c = A_1 \sin k\left(h - |z|\right)$$

$$+ \left\{\cos kz \cos k\left(h - h_0\right) - \cos kh - \sin kh_0 \sin k\left(h - |z|\right)\right\} Y_c E_{0z} / \left(k^2 \cos kh\right) \ , \ 0 < |z| < h_0$$

Once again the distribution is not strictly $\cos kh - \cos kz$, but near the even resonance $kh = (m - 1/2)\,\pi$ it becomes proportional to $\cos kz$, and the Y_{rad} terms can be used. The differential mode is again

$$I_d = A_0 \sin \gamma\left(h' - |z|\right)$$

and thus

$$\frac{dI_d}{dz} = -Y_d V_d = -\gamma A_0 \cos \gamma\left(h' - |z|\right) \operatorname{sgn}(z)$$

$$\frac{dI_c}{dz} = -Y_c V_c = -kA_1 \cos k\left(h - |z|\right) \operatorname{sgn}(z)$$

$$- \left\{\sin kz \cos k\left(h - h_0\right) - \sin kh_0 \cos k\left(h - |z|\right) \operatorname{sgn}(z)\right\} Y_c E_{0z} / \left(k \cos kh\right) \ , \ 0 < |z| < h_0$$

At the center we have

$$I_d(0) = A_0 \sin \gamma h'$$

$$I_c(0) = A_1 \sin kh - (1 - \cos kh_0)\,(Y_c/k)\,(E_{0z}/k)$$

$$V_d(-0) - V_d(+0) = -2\frac{\gamma}{Y_d} A_0 \cos \gamma h'$$

$$V_c(-0) - V_c(+0) = -2\frac{k}{Y_c} A_1 \cos kh + 2 \sin kh_0\,(E_{0z}/k)$$

The conditions at the center

$$V_d(-0) - V_d(+0) = \frac{1}{2}\left[I_c(0) + I_d(0)\right] Z_L = V_c(-0) - V_c(+0)$$

then determine the unknowns

$$-\frac{2\gamma}{Y_d} A_0 \cos \gamma h' = -\frac{2k}{Y_c} A_1 \cos kh + 2 \sin kh_0\,(E_{0z}/k)$$

$$= \frac{1}{2}\left[A_1 \sin kh - (1 - \cos kh_0)\,(Y_c/k)\,(E_{0z}/k) + A_0 \sin \gamma h'\right] Z_L$$

or

$$\left[\left(\frac{2k}{Y_c} + \frac{1}{2} Z_L \frac{kY_d}{\gamma Y_c} \tan \gamma h'\right) \cos kh + \frac{1}{2} Z_L \sin kh\right] A_1$$

$$= \frac{1}{2} Z_L \left[(1 - \cos kh_0) + \left(\frac{kY_d}{\gamma Y_c} \sin kh_0\right) \tan \gamma h'\right] (Y_c/k)\,(E_{0z}/k) + 2 \sin kh_0\,(E_{0z}/k)$$

$$A_0 \cos \gamma h' = \frac{kY_d}{\gamma Y_c} A_1 \cos kh - \frac{Y_d}{\gamma} \sin kh_0\,(E_{0z}/k)$$

The quantity of interest is the load current

$$I_+(0) = \frac{1}{2}\left[I_c(0) + I_d(0)\right]$$

$$= \frac{1}{2}\left[A_1 \sin kh - (1 - \cos kh_0)(Y_c/k)(E_{0z}/k) + A_0 \sin \gamma h'\right]$$

The power absorbed in the load, with

$$\mathrm{Re}(Z_L) = R_L$$

is then

$$P_{rec} = \frac{1}{2} R_L |I_+(0)|^2$$

We normalize here by

$$S_0 = \frac{1}{2}\eta_0 \left|H_y^{inc}\right|^2 = \frac{1}{2}\left|E_z^{inc}\right|^2/\eta_0 = \frac{1}{2\eta_0}|E_{0z}|^2$$

Approximate Antenna Problem We can simplify the preceding analysis for low impedance loads by subjecting the load to the short circuit current on the + wire (one half the common mode current) at the center of the cable. The antenna mode current without a load is

$$I_c = B\cos kz - (Y_c/k)(E_{0z}/k) \ , \ 0 < |z| < h_0$$

$$I_c = \left[B\cos kh_0 - (Y_c/k)(E_{0z}/k)\right]\sin k(h - |z|)/\sin k(h - h_0) \ , \ h_0 < |z| < h$$

Making the derivative continuous at $z = h_0$

$$(Y_c/k)(E_{0z}/k)\cos k(h - h_0) = B\left[\cos kh_0 \cos k(h - h_0) - \sin kh_0 \sin k(h - h_0)\right] = B\cos kh$$

Thus

$$I_c = (Y_c/k)(E_{0z}/k)\left[\cos k(h - h_0)\cos kz/\cos kh - 1\right] \ , \ 0 < |z| < h_0$$

$$I_c = (Y_c/k)(E_{0z}/k)\left[\cos k(h - h_0)\cos kh_0/\cos kh - 1\right]\sin k(h - |z|)/\sin k(h - h_0) \ , \ h_0 < |z| < h$$

Now the load current is

$$I_+(0) = \frac{1}{2}I_c(0) = \frac{1}{2}(Y_c/k)(E_{0z}/k)(\cos kh_0 - 1 + \tan kh \sin kh_0)$$

Figure 21 shows the susceptibility curves for the antenna-coupling model as the curves with solid circles. The approximate short-circuit current calculation (dashed curves) nearly overlays the more exact solution (solid curves) except for a minor blip at 10.17 MHz (and others at higher frequencies). The low-frequency slope is the same as the loop without an attached transmission-line load (the black curve) because the common-mode drive results from the fixed electric field of the incident plane wave E_{0z}, and hence the current is $I = O(Y_c E_{0z}) = O(\omega)$, and thus $P_{rec} = O(\omega^2)$. The black solid curve "shorted loop asymptotes" exhibited similar low-frequency behavior $P_{rec} = O(\omega^2)$ because the current $I = O(V_{oc}/R_L) = O(\omega)$ is proportional to ω, as a result of the induced loop voltage being proportional to ω.

5.3.3 Ground Plane Problem

Next let us consider the preceding case when a ground plane is present at a distance g below the cable. In this case the bulk or "common mode" transmission line equations become [11]

$$\frac{dV_c}{dz} = -Z_c I_c + K_m$$

$$\frac{dI_c}{dz} = -Y_c V_c + K$$

where the sources for $g >> a_{eq}$ are given by

$$K_m = -i\omega L^i H_y^{sc}$$

$$L^i \approx \mu_0 g$$

$$K \approx i\omega C^i E_x^{sc}$$

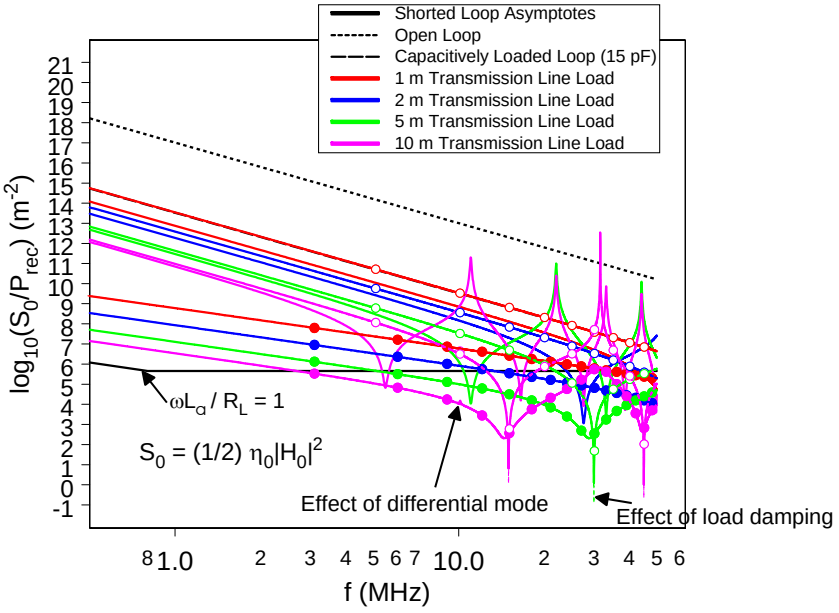

Figure 21. Susceptibility curves for antenna and transmission line coupling (in addition to the previous loop drives). The antenna results are the curves with solid circles. The drive existed over a one meter length at the antenna center. Each curve has a solid line, which includes the one ohm load self consistently, and a dashed line (nearly overlaying the other) which drives the one ohm load with the short circuit current. At 10.17 MHz you can see a slight upward blip in the 10 m curve, which indicates that the differential mode is diverting current around the one ohm load when it is included in the circuit, hence requiring a slightly higher drive field to achieve the same received power. The curves with the open circles are for the case where the transmission line is 0.1 m above a perfect ground plane. It is again driven over a one meter length at its center. There are solid curves which again include the one ohm load in the circuit, as well as dashed curves, which apply the short circuit current to the load (nearly overlaying the solid curves). Near the dips one can see the solid curves not going as low as the dashed curves because the damping from the low impedance load is having some effect in lowering the quality factor of the resonances, and possible diversion of current around the load due to the differential mode.

$$C^i \approx gC_{cm}$$

and E_x^{sc} and H_y^{sc} are the "short circuit" external fields in the presence of the ground plane. The impedance and admittance parameters are now

$$Z_c = \Delta Z_L - i\omega L_{cm}$$
$$Y_c = -i\omega C_{cm}$$

where now

$$k = \sqrt{-Z_c Y_c}$$

Notice that we can use Faraday's law

$$-\frac{\partial E_z^{sc}}{\partial x} + \frac{\partial E_x^{sc}}{\partial z} = i\omega\mu_0 H_y^{sc}$$

to show that

$$\frac{dV_c}{dz} = -Z_c I_c + g\frac{\partial E_z^{sc}}{\partial x} - g\frac{\partial E_x^{sc}}{\partial z}$$
$$\frac{dI_c}{dz} = -Y_c V_c - Y_c g E_x^{sc}$$

and thus

$$\left(\frac{d^2}{dz^2} + k^2\right) I_c = -Y_c g\frac{\partial E_z^{sc}}{\partial x}$$
$$\approx -Y_c \left[E_z^{sc}(x = g) - E_z^{sc}(x = 0)\right] = -Y_c E_z^{sc}(x = g)$$

and the final expression on the right is the result of using a finite-difference approximation for the short-circuit electric field derivative at low frequencies (noting that this field component vanishes on the ground plane). The correspondence with the preceding antenna equation (47) is apparent. For simplicity, here we take the electric field to be polarized in the z direction so that the only source term is K_m.

If we take twin 16 gauge wires ($2a \approx 0.051$") and a separation of $2h_w = 2.67\,(2a)$, with $g \approx 0.1$ m, $\ell_0 \approx 1$ m, and $\ell = 1$ m, 2 m, 5 m, 10 m, then

$$a_{eq} = \sqrt{ah_w} \approx 0.04167 \text{ in}$$
$$\Delta Z_L \approx \frac{1}{2}\frac{Z_s}{\pi a} \approx (1 - i)\frac{R_s}{2\pi a}$$

and in this case we use the approximate forms of the wire bundle above a ground plane

$$C_{cm} \approx \frac{2\pi\varepsilon_0}{\ln(2g/a_{eq})} \approx 10.61 \text{ pF/m}$$

$$L_{cm} \approx \frac{\mu_0}{2\pi}\ln(2g/a_{eq}) \approx 1.05\ \mu\text{H/m}$$

Eliminating the voltage in the transmission-line equations gives

$$\left(\frac{d^2}{dz^2} + k^2\right) I_c = -Y_c K_m\ ,\ 0 < |z| < \ell_0/2 = h_0$$

$$\left(\frac{d^2}{dz^2} + k^2\right) I_c = 0\ ,\ \ell_0/2 = h_0 < |z| < \ell/2 = h$$

and

$$I_c = A_1 \sin k\,(h - |z|)$$
$$+ \left\{\cos kz \cos k\,(h - h_0) - \cos kh - \sin kh_0 \sin k\,(h - |z|)\right\} Y_c K_m / \left(k^2 \cos kh\right)\ ,\ 0 < |z| < h_0$$
$$I_d = A_0 \sin\gamma\,(h' - |z|)$$

The matching equations and current $I_+(0)$ are identical to those in the preceding antenna section (only Y_c, Z_c, k, and $E_{0z} \to K_m$ are different). The same holds for the approximate solution using the short circuit current. These results are shown as the curves with open circles in Fig. 21. We normalize here by

$$S_0 = \frac{1}{2}\eta_0 \left|H_y^{sc}\right|^2$$

Again there are two sets of curves with open circles, associated with the ground plane, the solid curves include the load in the circuit, whereas the dashed curves use the short circuit current through the load.

Notice that the approximate solution (dashed curves) nearly overlays the more exact solution (solid curves) except at the resonance minimums, where the extra damping from the load raises the bottoms of the solid curves (and it is possible that there is some diversion of current around the load due to the differential mode). The low-frequency slope here is the same as the open circuited loop because the reflection of the incident field in the nearby ground plane introduces an extra factor of frequency in the common mode current $I = O\left(Y_c K_m\right) = O\left(\omega^2\right)$, and thus $P_{rec} = O\left(\omega^4\right)$. The black dashed curve "open loop" of Figure 21 (along with the 15 pF load, shown as long black dashes, and the transmission line loads, shown as solid color curves without circles) all show a similar behavior because $I = O\left(V_{oc}\omega C_a\right) = O\left(\omega^2\right)$ and hence $P_{rec} = O\left(\omega^4\right)$.

6 CONCLUSIONS

This report estimates inductively coupled energy to a low impedance load in a loop-to-loop arrangement. The transmitter loop is taken to be either a circular geometry or a rectangular-loop (stripline-type) geometry that was used in an experimental setup. Simple magnetic field models are constructed and used to estimate the mutual inductance to the receiving loop, which is taken to be circular with one or several turns. Circuit elements are estimated and used to determine the coupled current and power (an equivalent antenna picture is also given). These results are compared to an electromagnetic simulation of the transmitter geometry. Simple approximate relations are also given to estimate coupled energy from the power. The effect of additional loads in the form of attached leads, forming transmission lines, are considered. The results are summarized in a set of susceptibility-type curves. Finally, we also consider drives to the cables themselves and the resulting common-to-differential mode currents in the load.

7 REFERENCES

[1] S. Ramo, J. R. Whinnery, and T. Van Duzer, **Fields and Waves in Communication Electronics**, New York: John Wiley & Sons, Inc., 1965, pp. 306-311, Table 8.09.

[2] P. D. Coleman and L. D. Lucero, Private Communication, Dec. 2011.

[3] L. K. Warne, R. E. Jorgenson, R. S. Coats, L. E. Martinez, J. M. Jojola, S. L. Montoya, K. O. Merewether, and E. Bystrom, "Protection Characteristics of a Faraday Cage Compromised by Lightning Burnthrough," Sandia National Laboratories Report, SAND2012-0040, January, 2012, p. 86.

[4] W. R. Smythe, **Static and Dynamic Electricity**, New York: Hemisphere Pub. Corp., 1989, Ch. IV.

[5] I. S. Gradshteyn and I. M. Ryzhik, **Tables of Integrals, Series, and Products**, New York: Academic Press, 1965, pp. 89, 90, 366.

[6] F. W. Grover, **Inductance Calculations**, New York: Dover Pub., Inc., 1962, Ch. 16, p. 60.

[7] S. A. Schelkunoff, **Antenna Theory and Practice**, New York: John Wiley & Sons, Inc., 1952, pp. 179-180, 319-322, 506.

[8] K. S. H. Lee and F. C. Yang, "Trends and Bounds in RF Coupling to a Wire Inside a Slotted Cavity," IEEE Trans. on Electromagnetic Compat., Vol. 34, No. 3, Aug. 1992, pp. 154-160.

[9] L. K. Warne and K. C. Chen, "Long Line Coupling Models," Sandia National Laboratories Report, SAND2004-0872, March 2004.

[10] L. K. Warne and K. C. Chen, "A Simple Transmission Line Model for Narrow Slot Apertures Having Depth and Losses," IEEE Trans. on Electromag. Compat., Vol. 34, No. 3, Aug. 1992, pp. 173-182.

[11] K. S. H. Lee (editor), **EMP Interaction: Principles, Techniques, and Reference Data**, Washington: Hemisphere Pub. Co., 1986, Sections 1.3.2 and 2.4.2.

DISTRIBUTION

Number	Mail Stop	Name	Dept.
1 (electronic)	MS1152	M. Caldwell	1652
1	MS1152	L. I. Basilio	1652
1	MS1152	W. L. Langston	1652
2	MS1152	L. K. Warne	1652
1 (electronic)	MS1178	M. L. Kiefer	1653
1	MS1152	R. A. Salazar	1653
1 (electronic)	MS1173	J. A. Alexander	5443
1	MS1173	L. D. Bacon	5443
1	MS1173	P. D. Coleman	5443
1	MS1173	L. M. Lucero	5443
1	MS1173	J. T. Williams	5443
1 (electronic)	MS0899	Technical Library	9536


Sandia National Laboratories